Am J Transl Res 2022;14(9):6504-6520
www.ajtr.org /ISSN:1943-8141/AJTR0144013

Original Article

Comprehensive analysis of N6-methyladenosine-related lncRNAs reveals distinct hepatocellular carcinoma subtypes with immunotherapeutic implications

Xiaodong Xie[1,2], Hongyin Liang[1,2], Qing Ruan[1,2], Xiao Ma[1,2], Chuan Xie[1,2], Zhulin Luo[1,2], Lijun Tang[1,2], Long Cheng[1,2], Tao Wang[1,2]

[1]Department of General Surgery, The General Hospital of Western Theater Command (Chengdu Military General Hospital), Chengdu 610083, Sichuan Province, China; [2]Department of General Surgery and Pancreatic Injury and Repair Key Laboratory of Sichuan Province, The General Hospital of Western Theater Command (Chengdu Military General Hospital), Chengdu 610083, Sichuan Province, China

Received May 9, 2022; Accepted August 2, 2022; Epub September 15, 2022; Published September 30, 2022

Abstract: Accumulating studies have demonstrated critical roles of N6-methyladenosine (m6A) modification and long noncoding RNAs (lncRNAs) in the biological processes leading to occurrence, development and chemoresistance of cancers. However, the specific identities and functional roles of lncRNAs associated with m6A modification in hepatocellular carcinoma (HCC) remain elusive. In this study, eighty-two prognostic m6A-related lncRNAs (m6A-LncRNAs) were identified in HCC datasets. Patients with HCC were classified into three subtypes (C1, C2 and C3) based on the expression of the m6A-LncRNAs. The three subtypes showed significant differences in clinical features, immune and stromal infiltration signatures, and immunotherapy sensitivity. Subclass C1 was notable for high immune and stromal cell infiltration and active immune responses, low serum α-fetoprotein (AFP) levels and high sensitivity to immune checkpoint inhibitors (ICIs). Subclass C2 showed high metabolic activities and absence of immune infiltration with favorable prognosis. Subclass C3 was associated with an exhausted immune environment, high serum AFP and poor prognosis. Notably, subclass C3 displayed high expression of immune checkpoints but failed to respond to ICIs. Finally, 12 m6A-LncRNA signatures were identified for HCC classification and validated in an external dataset. This integrated analysis indicated that the interactions between m6A methylation and lncRNAs are involved in immune and stromal cell infiltration in HCC, and may provide novel insights into precision diagnostics as well as therapeutics for HCC patients.

Keywords: M6A, hepatocellular carcinoma, immune microenvironment

Introduction

Liver cancer represents one of the most prevalent malignant tumors in the world. It was estimated that there were 905,677 new liver cancer cases and 830,180 liver cancer-related deaths globally in 2020. The World Health Organization (WHO) estimates that in 2030, more than 1 million patients will die from liver cancer [1, 2]. Hepatocellular carcinoma (HCC), accounting for 75-85% of liver cancer cases, was usually secondary to chronic infection with hepatitis B virus (HBV) or hepatitis C virus (HCV), alcoholic and nonalcoholic hepatitis, aflatoxin-contaminated foodstuffs and metabolic disorders. Despite great advances in HCC treatment over the past few decades, the 5-year survival rate of HCC is approximately 18%, which makes liver cancer the second most lethal common tumor [3].

N6-methyladenosine (m6A) modification has been identified to play vital roles in many critical cellular processes such as cell proliferation, differentiation and apoptosis [4]. The m6A modification process is regulated by 3 main groups of molecular components: methyltransferases ("writers"), demethylases ("erasers"), and recognition factors ("readers") [5]. Recently, several of these elements responsible for regulation of m6A modification in oncogenesis and progression in HCC have been identified [6].

WTAP contributes to HCC progression via the HuR-ETS1-p21/p27 axis [7]. METTL14 suppresses the metastatic potential of HCC by regulating the EGFR/PI3K/AKT signaling pathway [8]. However, additional roles of m6A modification in HCC remain uncovered.

Emerging evidence has suggested that dysregulated long non-coding RNAs (lncRNAs) participate in various cancerous phenotypes such as persistent proliferation and evasion of apoptosis [9, 10]. In the context of other tumors, m6A modification of lncRNAs have been shown to play key mechanistic roles [11]. For instance, YTHDF3 modification of lncRNA GAS5 alters its degradation rate and facilitates colorectal cancer (CRC) progression both in vitro and in vivo. METTL14 downregulates lncRNA XIST and suppresses the proliferation and metastasis of CRC. In the context of HCC, METTL3-related m6A modification of LINC00958 stabilizes the transcripts and upregulates its expression, which promotes the expression of hepatoma-derived growth factors and facilitates HCC lipogenesis and progression [12]. Further clarification of additional mechanisms underlying the m6A modification and HCC-related lncRNAs may thus help to elucidate new molecular mechanisms of HCC and identify therapeutic biomarkers and targets for intervention.

Here, we identified 82 m6A-related lncRNAs (m6A-LncRNAs) with prognostic significance in HCC and constructed an m6A-lncRNA regulatory network. Based on the expression of the prognostic m6A-LncRNAs, we discovered three molecular HCC subtypes with distinct clinical features, immune and stromal infiltration signatures and immunotherapy sensitivity.

Materials and methods

Data acquisition and preprocessing

The fragments per kilobase of transcript per million mapped reads (FPKM) normalized expression files, annotated somatic mutation files and clinical information of HCC patients were obtained from the TCGA Data Portal (https://portal.gdc.cancer.gov/). Another 161 gene expression files of HCC patients from the ICGC database (https://dcc.icgc.org/) were also included in this study. All gene expression data in the TCGA and ICGC datasets were annotated based on the GENCODE project (http://www.gencodegenes.org). A total of 19,505 mRNAs and 15,253 lncRNAs were identified in the TCGA dataset, and 19,913 mRNAs and 13,081 lncRNAs were identified in the ICGC dataset. For the duplicated samples and genes with multiple transcripts, the average value was taken as the expression level.

Identification of m6A-LncRNAs

Based on previous studies, the expression matrix of m6A regulatory genes was extracted from the TCGA and ICGC datasets, including the readers (YTHDF1, YTHDF2, YTHDF3, YTHDC1, YTHDC2, IGF2BP1, IGF2BP2, IGF2BP3, FMR1, LRPPRC, HNRNPC, HNRNPA2B1 and RBMX), writers (WTAP, VIRMA, ZC3H13, RBM15, RBM15B, METTL3, METTL14 and METTL16) and erasers (FTO and ALKBH5) [13, 14]. Pearson correlation analysis was first implemented between m6A genes and all lncRNA expression data in the two datasets. The intersecting lncRNAs in the two datasets with absolute correlation > 0.3 and p value < 0.001 were identified as possible m6A-LncRNAs. Cox regression analysis was implemented to filter the prognostic m6A-LncRNAs (p value < 0.05). The correlation network was constructed using Cytoscape (version 3.7.2) software.

Identification and characterization of HCC subclasses

The non-negative matrix factorization (NMF) algorithm, which decomposes the original matrix with non-negative elements into two non-negative matrices, is an effective dimension reduction method for high dimension data, and has been frequently applied for clustering gene expression profiles [15, 16]. NMF was performed using the R package “NMF” (version 0.23.0). The standard NMF algorithm with ‘brunet’ criterion was selected for the method, and 50 iterations were carried out. To estimate the optimal factorization rank, the rank k was set as parameter tested from 2 to 10, and the optimal rank was chosen when the cophenetic correlation coefficient started to decline. k=3 was selected as the optimal k value, indicating that the HCC samples can be well clustered into 3 clusters. To identify the hub m6A-LncRNAs, we extracted the top N m6A-LncRNA contributing features of each cluster based on feature scores implemented by the NMF algorithm and evaluated with principal component analysis

(PCA). The minimum numbers of lncRNAs necessary for differentiating between identified three HCC subclasses were considered to be hub m6A-LncRNAs. Subsequently, the three clusters can be clearly distinguished with the top 5 contributing lncRNAs. We then validated the 5 selected lncRNAs in an external dataset. The R package "survival" (version 3.1-7) was used to compare the overall survival (OS) and disease-free survival (DFS) between the different clusters through Kaplan-Meier analysis. The R package "maftools" (version 2.2.10) was used to visualize the gene mutation and copy number alteration for each subtype.

Tumor microenvironment analysis

As previously described, to score the relative abundance of immune and stromal cells in tumors, the whole-tumor gene expression data was examined with the xCell algorithm web server (https://xcell.ucsf.edu/) [17]. The QuantiSeq algorithm was used to quantify the absolute fraction of immune cells [18]. The cytotoxic activity of immune cells was calculated through the average expression of five granzymes (GZMA, GZMB, GZMH, GZMK, and GZMM) and the key cytolytic protein perforin-1 (PRF1). Tumor inflammation scores were computed based on the 18-gene signature as previously described [19].

Functional analysis

To investigate the variation in biological processes between the different HCC clusters, gene set variation analysis (GSVA) was utilized against the hallmark gene set with the R package "GSVA" (version 1.34.0) [20]. The differentially expressed genes (DEGs) between the three clusters (C1 vs. C2, C2 vs. C3, C1 vs. C3) were calculated with "DEseq2" with the filter |log2 (fold change)| > 2 and adjust p value < 0.05. These DEGs were then used for enrichment analysis with Metascape, which provides mainstream ontology terms, including gene ontology (GO) processes, KEGG pathways, canonical pathways, Reactome gene sets and CORUM complexes [21, 22].

Prediction of the response to immune checkpoint inhibitors (ICIs) and targeted drugs

The Tumor Immune Dysfunction and Exclusion (TIDE) and Immunophenoscore (IPS) algorithms were utilized to predict the response to ICIs [23, 24]. TIDE assesses immune evasion mechanisms, including the induction of T cell dysfunction and the prevention of T cell infiltration. IPS identified determinants of tumor immunogenicity and described the cancer antigenomes and immune landscapes and is a superior predictor of the response to CTLA4 and PD-1 blockades. The similarity of gene expression profiles between our HCC subclasses and melanoma patients treated with ICIs was calculated to indirectly predict the immunotherapy efficacy based on SubMap analysis (Gene Pattern) [25]. The R package "pRRophetic" (version 0.5) was used to predict the clinical chemotherapeutic responses [26].

Statistical analysis

All statistical data were analyzed in the R environment (R version: 3.6.3). Unpaired Student's t-test was used to estimate the statistical significance of normally distributed variables, while the Wilcoxon rank-sum test was used to analyze the statistical significance of non-normally distributed variables. Kaplan-Meier analyses and log-rank tests were performed to assess the survival difference between clusters. Multivariate Cox regression analyses were calculated to identify factors with independent prognostic value. A P-value less than 0.05 was regarded as statistically significant.

Results

Identification of m6A-LncRNAs in patients with HCC

The expression matrix of 23 m6A RNA methylation regulatory genes and total lncRNAs were extracted from the TCGA and ICGC datasets. Through Pearson correlation analysis of the m6A regulatory genes and lncRNAs, we identified 3,567 m6A-LncRNAs in the TCGA datasets and 4,243 m6A-LncRNAs in the ICGC dataset (|Cor| > 0.3 and P < 0.001). Ultimately, the 850 lncRNAs with expression files closely correlated to m6A methylation and conserved in both datasets were defined as m6A-LncRNAs. Compared with normal tissues, most of these m6A-LncRNAs showed enriched expression in tumor tissues (**Figure 1A**). The locations of m6A-LncRNAs on chromosomes are shown in Figure S1. To obtain prognostic m6A-LncRNAs, univariate Cox regression analysis was imple-

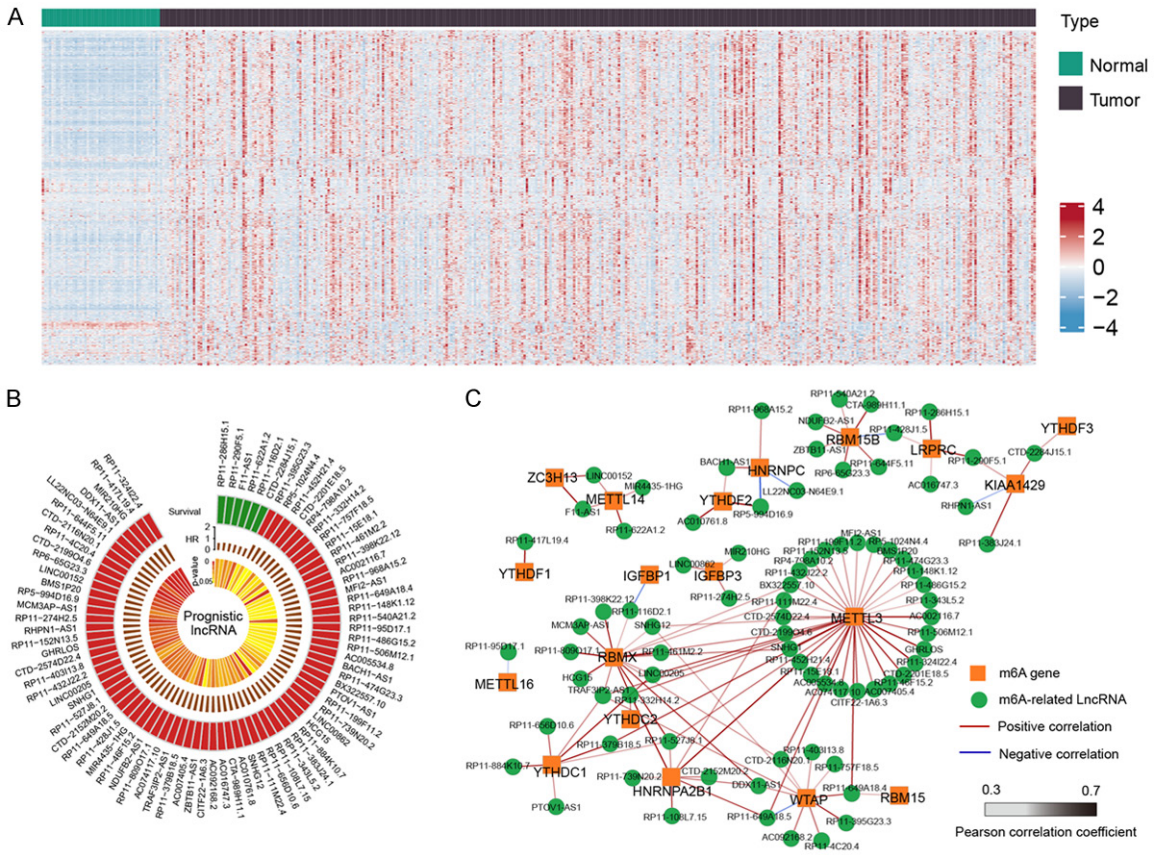

Figure 1. Identification of m6a-related lncRNAs (m6A-LncRNAs). A. Heatmap of m6A-LncRNAs in hepatocellular carcinoma (HCC) and normal tissue. B. Circle plot of the 82 prognostic m6A-LncRNAs. Green, protective factors; red, risk factors. C. Regulatory network of the m6A (N6-methyladenosine) genes and m6A-LncRNAs.

mented on 850 m6A-LncRNAs combined with prognostic information. Eighty-two prognostic m6A-LncRNAs were identified to be significantly correlated with the OS of HCC patients (FDR < 0.05), including 6 protective lncRNAs and 76 risk lncRNAs (**Figure 1B** and Table S1). The correlation network between m6A genes and prognostic m6A-LncRNAs is shown in **Figure 1C** and Table S2.

M6A-LncRNAs characterized HCC patients into three subtypes with distinct clinical outcomes

To further explore the roles of m6A-LncRNAs in HCC, 82 prognostic m6A-LncRNAs were included for NMF consensus clustering analysis. Based on the cophenetic correlation coefficients, k=3 was selected as the optimal k value; thus, the HCC patients were grouped into 3 clusters (**Figure 2A**), including 84 cases in cluster 1 (C1), 170 cases in cluster 2 (C2) and 117 cases in cluster 3 (C3). The prognostic m6A-LncRNAs had significantly different expression panels in the three clusters, and most of the lncRNAs had the highest expression in cluster 3 (**Figure 2B**). Interestingly, C2 exhibited the best rates of overall survival (OS) and disease-free survival (DFS), whereas C3 displayed the worst prognosis (P < 0.001, **Figure 2C** and **2D**). Serum alpha fetoprotein (AFP) is a commonly used clinical marker for HCC surveillance. In comparison with the other two clusters, C3 had the highest serum AFP levels (C1 vs. C2, no significance; C2 vs. C3, P < 0.0001; C1 vs. C3, P < 0.0001; **Figure 2E**). Moreover, patients in C3 typically presented an advanced clinical stage and pathological stage (P < 0.0001, **Figure 2F** and **2G**). To evaluate whether the clusters characterized by the m6A-LncRNAs had independent prognostic value, we performed multivariate Cox regression analysis with multiple clinical and pathological factors. After adjusting for age, sex, grade and stage, this classification remained statistically significant (C1 vs. C2, HR,

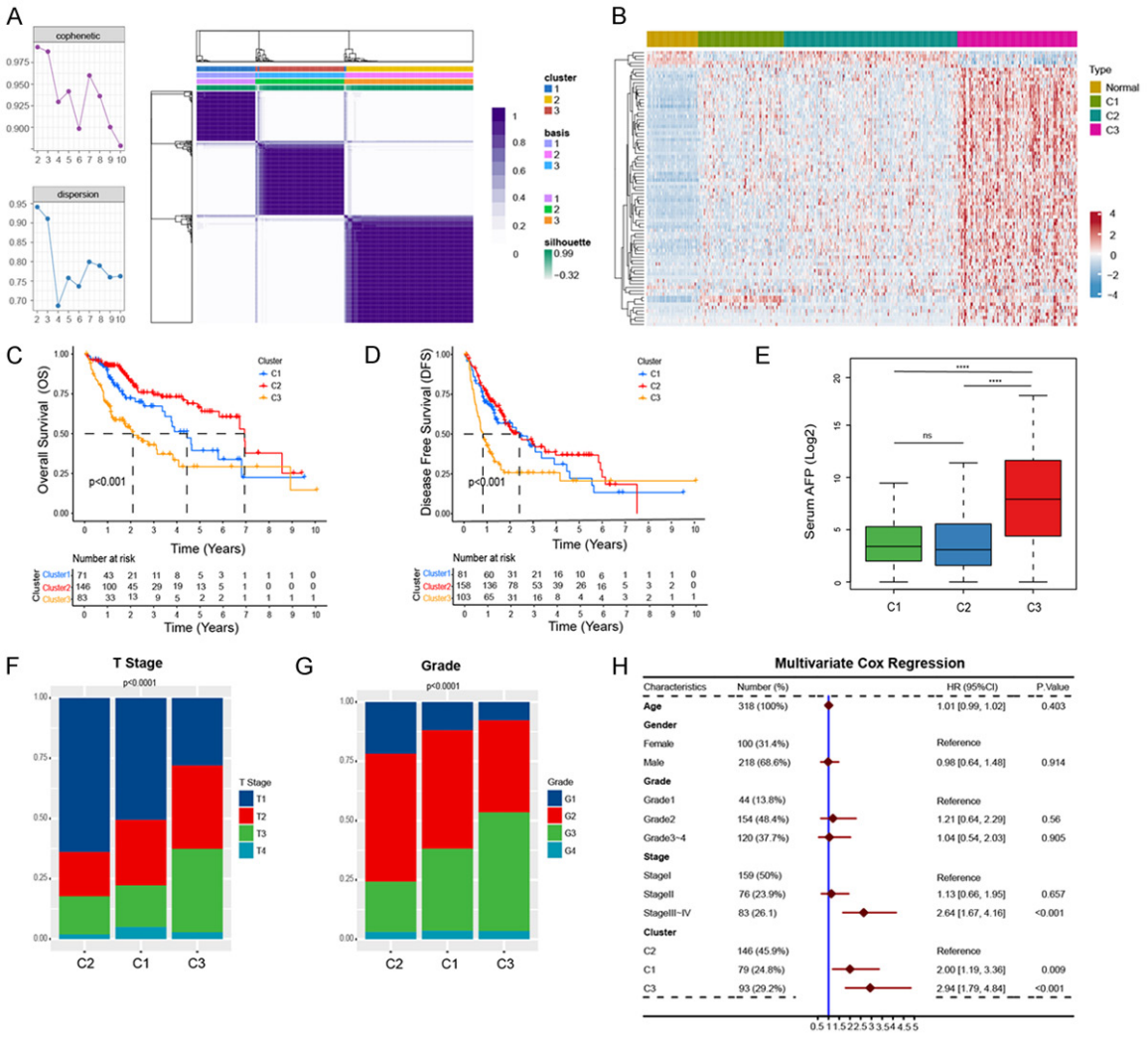

Figure 2. Identification of HCC subclasses with the non-negative matrix factorization (NMF) consensus clustering algorithm. A. NMF clustering based on 82 prognostic m6A-LncRNAs. The cophenetic correlation coefficient is shown for k=2-10. B. Heatmap of the 82 prognostic m6A-LncRNAs in normal tissue and the three HCC subclasses. C. Kaplan-Meier analysis of overall survival (OS). D. Disease-free survival (DFS) of the three subclasses. The statistical significance of differences was determined by the log-rank test. E. Comparison of the serum alpha fetoprotein (AFP) level of the three subclasses. F, G. Comparison of the fractions of T stage and grade of the three subclasses. H. Multivariate Cox regression analysis with multiple clinical and pathological factors. Statistical significance of differences was determined by Wilcoxon rank-sum test. *, P < 0.05; **, P < 0.01; ***, P < 0.001; ****, P < 0.0001; ns, no significance.

2.00 [95% CI, 1.19 to 3.36]; C3 vs. C2, HR, 2.94 [95% CI, 1.79 to 4.84]; **Figure 2H**).

The three clusters differ in somatic mutations and biological functions

In C3, 55% of the patients had TP53 mutations; however, only 17% and 23% of the patients had TP53 mutations in C2 and C1, respectively. In C1 and C2, CTNNB1 ranked as the most frequently mutated gene, accounting for 29% of mutations, while only 17% of CTNNB1 mutated in C3 tumors (**Figure 3A**). Several recent studies have demonstrated that tumor mutation burden (TMB) and neoantigen load correlate with immune infiltration and response to immunotherapy [27, 28]. However, no significant difference was identified for either TMB or the number of putative neoantigens in comparison between the three subtypes (**Figure 3B**). In terms of somatic copy number variation (CNV), patients in C3 showed a higher total CNV number than those in C2 and C1 (C2 vs. C1, no significance; C2 vs. C3, P < 0.0001; C1 vs. C3, P <

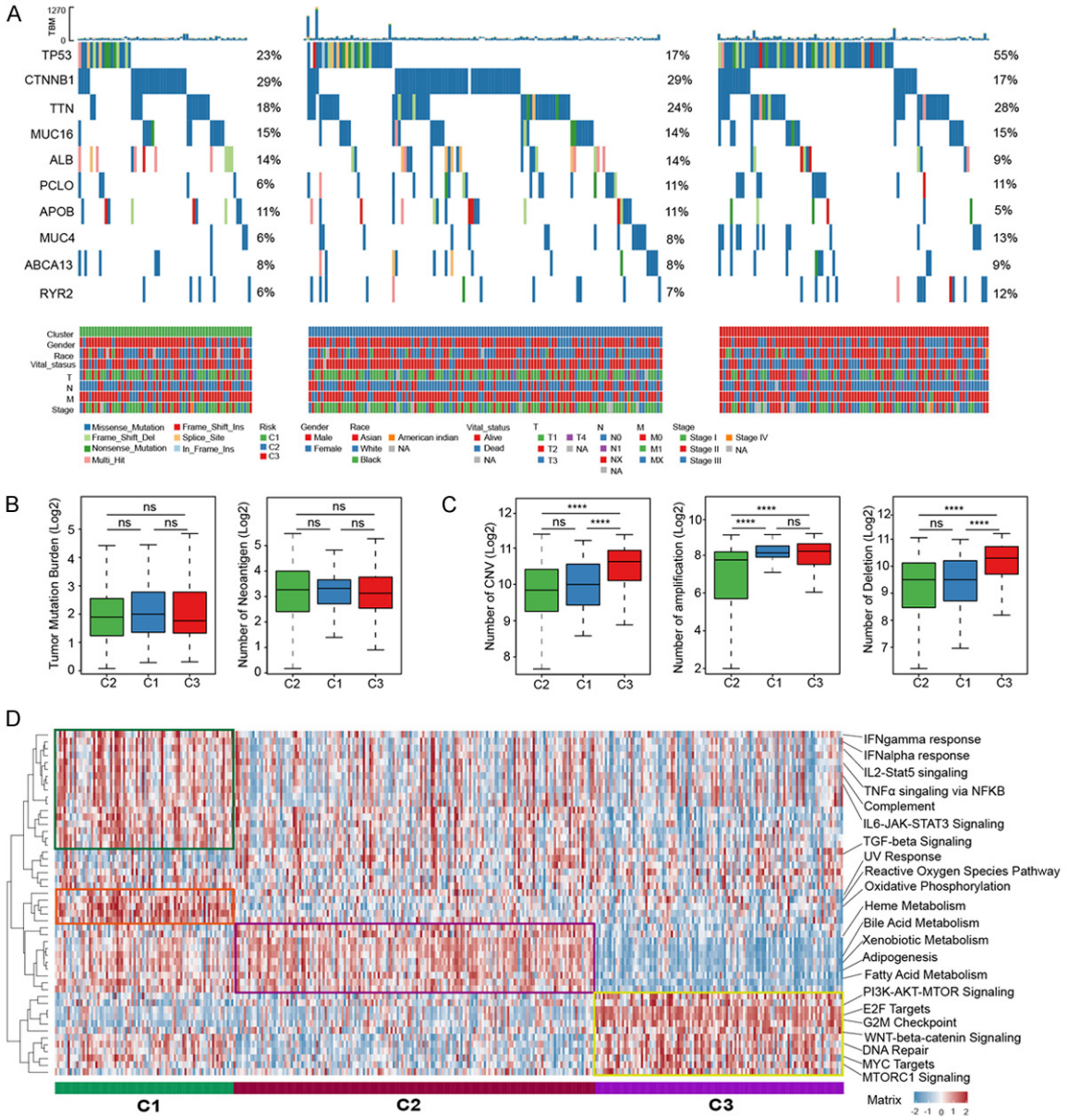

Figure 3. Somatic mutation and biological function analysis of three HCC subclasses. A. Waterfall plot of high-frequency mutated genes in the three subclasses. B. Comparison of tumor mutation burden (TMB) and neoantigens in the three subclasses. C. Total copy number variation (CNV), amplification and deletion of the three subclasses. D. Heatmap of geneset variation analysis (GSVA) of the hallmark gene set. Statistical significance of differences was determined by Wilcoxon rank-sum test. *, P < 0.05; **, P < 0.01; ***, P < 0.001; ****, P < 0.0001; ns, no significance.

0.0001). C1 and C3 showed higher copy number amplification (C2 vs. C1, P < 0.0001; C2 vs. C3, no significance; C1 vs. C3, P < 0.0001), and C3 also showed higher copy number deletion (C2 vs. C1, no significance; C2 vs. C3, P < 0.0001; C1 vs. C3, P < 0.0001; **Figure 3C**).

To investigate the crucial biological processes involved in m6A-LncRNA modification patterns between the clusters, GSVA enrichment analysis was performed against the hallmark gene set. GSVA analysis indicated that C2 was mainly enriched in metabolic-related pathways, such as bile/fatty acid metabolism, heme metabolism and adipogenesis. C3 was highly enriched in DNA repair, cell proliferation and immunosuppression related pathways, such as G2M checkpoints, E2F targets, MYC targets and

TGFβ signaling pathways. The C1 subtype was significantly enriched in inflammatory and activated immune processes and mitochondrial stress, including IFN alpha/gamma response, IL2-Stat5 and IL6-Jak-Stat5 signaling and reactive oxygen species pathway and oxidative phosphorylation (**Figure 3D** and Table S3). We then analyzed the differentially expressed genes (DEGs) [|log2 (fold change)| > 2 and p.adj < 0.05] between the three clusters. A total of 204 DEGs between C1 and C2, 647 DEGs between C1 and C3 and 1,040 DEGs between C2 and C3 were identified. These DEGs were then used for enrichment analysis with Metascape, which provides mainstream ontology terms, including KEGG pathways, gene ontology (GO) processes, canonical pathways, reactome gene sets, CORUM complexes, etc. The DEGs between C1 and C2 were mainly enriched in neuroactive ligand-receptor interactions and organic hydroxy compound transport. The DEGs between C2 and C3 were mainly enriched in NABA matrisome association, regulation of hormone levels and metapathway biotransformation phase I and II. The DEGs between C1 and C3 were mainly enriched in matrisome association and embryonic morphogenesis (Figure S2).

The three clusters showed distinct immune and stromal infiltration signatures

Considering significant differences have been identified in proliferation, immunity and metabolism related pathways among the 3 clusters, we then examined the distribution of stromal and immune content of each cluster through the xCell algorithm, which characterized 64 immune and stromal cells spanning multiple adaptive and innate immune cells, epithelial cells, extracellular matrix cells, and hematopoietic progenitors derived from thousands of expression profiles [17]. As a result, C2 showed a signature of low immune cell prevalence and high stromal cell infiltration, while C3 showed high immune cell and low stromal cell content, and C1 showed both high immune cell and stromal cell infiltration (**Figure 4A**). C1 and C3 had higher overall immune scores (C2 vs. C1, P < 0.0001; C2 vs. C3, P < 0.0001; C1 vs. C3, no significance), and C1 and C2 showed higher stromal scores (C2 vs. C1, no significance; C2 vs. C3, P < 0.0001; C1 vs. C3, P < 0.0001; **Figure 4B** and **4C**). Cytolytic responses provide an active defense against tumors. The average expression of granzymes (*GZMA, GZMB, GZMH, GZMK, and GZMM*) and *PRF1* was quantified to examine the cytolytic (CYT) activity in the three clusters. Consistent with the immune scores, the CYT scores of C1 and C3 were significantly higher than that of C2 (C2 vs. C1, P < 0.0001; C2 vs. C3, P < 0.01; C1 vs. C3, no significance; **Figure 4D**). We further calculated the tumor inflammation score (TIS) and found that C1 and C3 presented higher inflammatory scores than C2 (C2 vs. C1, P < 0.0001; C2 vs. C3, P < 0.01; C1 vs. C3, no significance; **Figure 4E**).

To further validate the immune infiltration pattern, we computed the immune content by the quantiSeq algorithm, which provides an 'absolute score' of the cell fraction and has good accuracy for the estimation of immune cell infiltration in bulk RNA-seq data [29]. C3 had higher B cell (C2 vs. C1, P < 0.05; C2 vs. C3, P < 0.0001; C1 vs. C3, P < 0.0001), M1 macrophage (C2 vs. C1, P < 0.05; C2 vs. C3, P < 0.001; C1 vs. C3, no significance), M2 macrophage (C2 vs. C1, no significance; C2 vs. C3, P < 0.001; C1 vs. C3, P < 0.0001), $CD8^+$ T cell (C2 vs. C1, P < 0.01; C2 vs. C3, P < 0.01; C1 vs. C3, P < 0.0001) and regulatory T cell (C2 vs. C1, no significance; C2 vs. C3, P < 0.0001; C1 vs. C3, P < 0.0001) infiltrate fractions , while C2 had higher NK cell recruitment (C2 vs. C1, P < 0.05; C2 vs. C3, P < 0.001; C1 vs. C3, no significance; **Figure 4F**). To ensure the robustness of these analyses, we further repeated these calculations using the TIMER and MCPcounter algorithms, leading to qualitatively similar results (Figure S3). We then detected the expression of cell exhaustion related genes in the 3 clusters, and found that C3 subtype had significant higher expression of cell exhaustion markers, such as *PD-L1, CTLA4, TIGIT, LAG3, PD1* and *HAVCR2* (**Figure 4G**).

Identification and validation 12 m6A-LncRNA signatures for the three clusters

To better assess the roles of the m6A-LncRNAs in HCC, we extracted the top 5 contributing features of each cluster based on feature scores implemented by the NMF method, and we obtained 12 m6A-LncRNA signatures for the three clusters (**Table 1**). These features had significantly different expression patterns in different groups (**Figure 5A**). Subsequently,

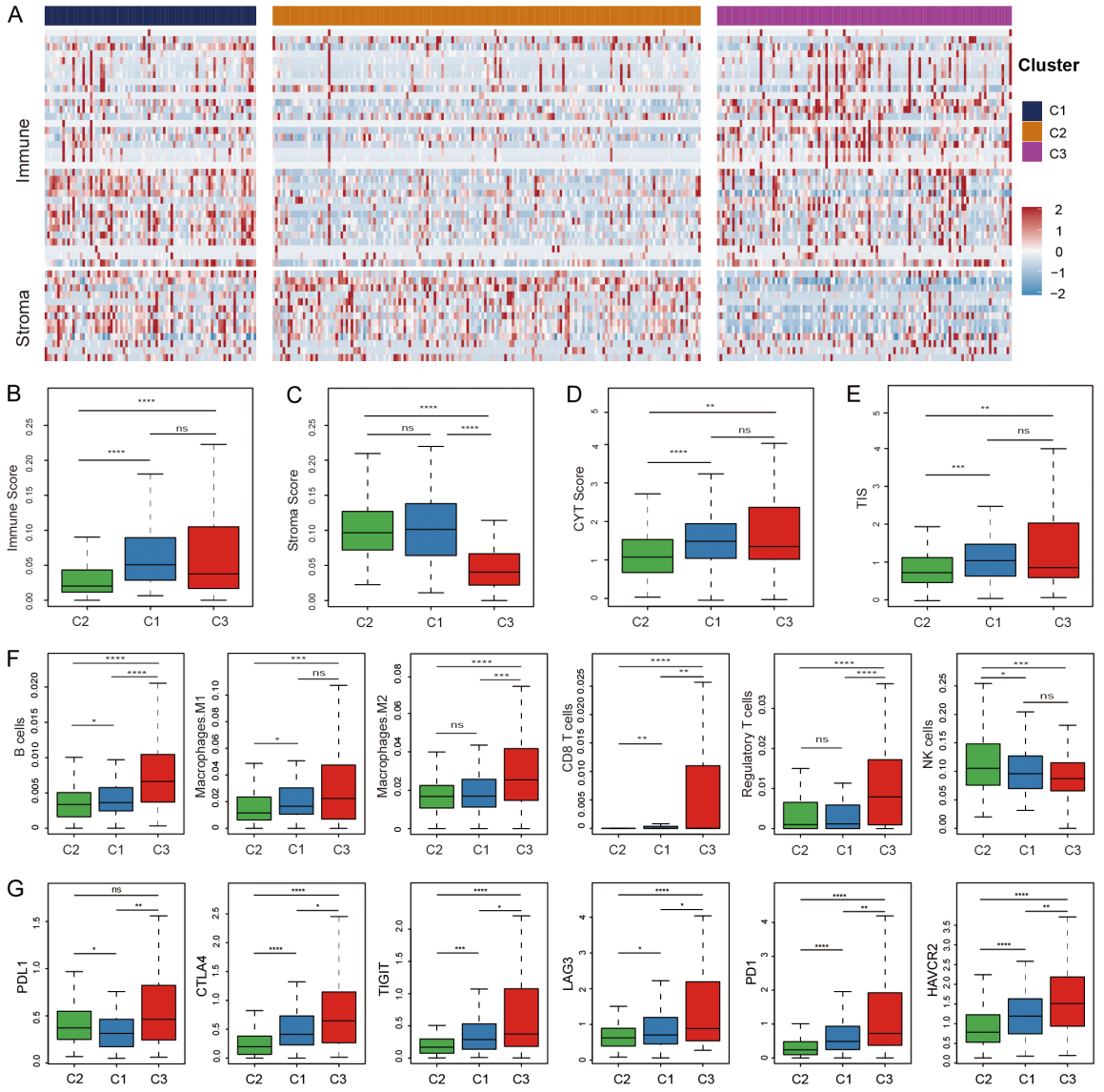

Figure 4. Tumor microenvironment (TME) characteristics of the three HCC subclasses. A. Heatmap of the cell infiltration score calculated with the xCell algorithm. Red indicates higher score, and blue indicates lower score. B-E. Comparison of immune score, stroma score, tumor inflammation score (TIS) and cytolytic (CYT) score of the three subclasses. F. Absolute fraction of immune cell population in each subclass determined using quantiseq. G. Comparison of the expression of checkpoint genes in the three subclasses. Statistical significance of differences was determined by Wilcoxon rank-sum test. *, P < 0.05; **, P < 0.01; ***, P < 0.001; ****, P < 0.0001; ns, no significance.

Table 1. Top5 contributive signatures for the 3 clusters

C1	C2	C3
RP11-116D2.1	RP11-116D2.1	SNHG12
LINC00152	RP11-622A1.2	MIR210HG
MIR4435-1HG	F11-AS1	LINC00205
SNHG1	RP11-290F5.1	SNHG1
RP11-644F5.11	CTD-2284J15.1	RP11-644F5.11

based on the 12 signatures, the three clusters can be clearly distinguished with principal component analysis (PCA) (**Figure 5B**). Five of the lncRNAs showed protective potential, and the remaining 7 lncRNAs were risk factors (**Figure 5C**).

To validate the 12 signatures in external data, expression spectra of the 12 lncRNAs were extracted in the ICGC dataset. Unsupervised clustering was conducted based on the NMF algorithm. Consistent with the TCGA dataset, the ICGC validation dataset was clustered into three groups (**Figure 6A** and **6B**): 74 HCC patients in Cluster 1, 46 HCC patients in Cluster

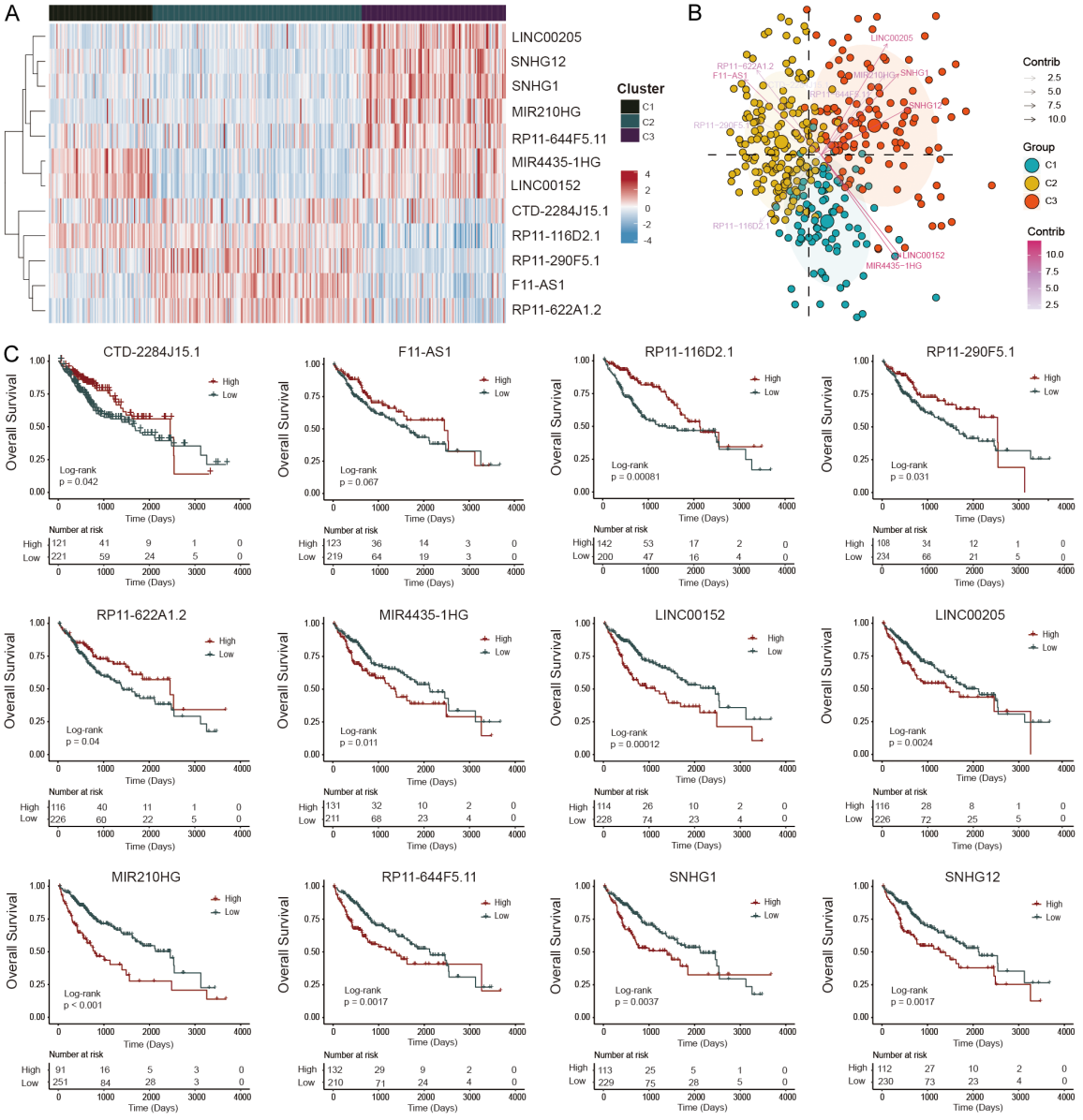

Figure 5. Identification of the contributive signatures for the three clusters. A. Heatmap of the expression of the 12 contributive lncRNAs for the three clusters. B. Internal validation of the classification based on the 12 lncRNAs using principal component analysis (PCA). C. Kaplan-Meier analysis of the 12 lncRNAs in the three subclasses. The statistical significance of differences was determined by the log-rank test.

2 and 41 HCC patients in Cluster 3. The expression pattern of the 12 lncRNAs was similar to that of the TCGA dataset (**Figure 6C**). We then analyzed immune infiltration in the three subtypes and found high immune infiltration and a low stromal infiltration signature in Cluster 3, which was consistent with the TCGA dataset (**Figure 6D** and **6E**). Furthermore, the absolute immune cell fraction score was calculated with the quantiSeq algorithm, and we found that Cluster3 had higher B cell (Cluster1 vs. Cluster2, $p < 0.05$; Cluster1 vs. Cluster3, no significance; Cluster2 vs. Cluster3, $P < 0.001$), M1 macrophage (Cluster1 vs. Cluster2, no significance; Cluster1 vs. Cluster3, $P < 0.0001$; Cluster2 vs. Cluster3, $P < 0.001$), M2 macrophage (Cluster1 vs. Cluster2, no significance; Cluster1 vs. Cluster3, $p < 0.0001$; Cluster2 vs. Cluster3, $P < 0.001$), CD8 T cell M1 macrophage (Cluster1 vs. Cluster2, no significance; Cluster1 vs. Cluster3, $P < 0.0001$; Cluster2 vs. Cluster3, $P < 0.001$), and regulatory T cell

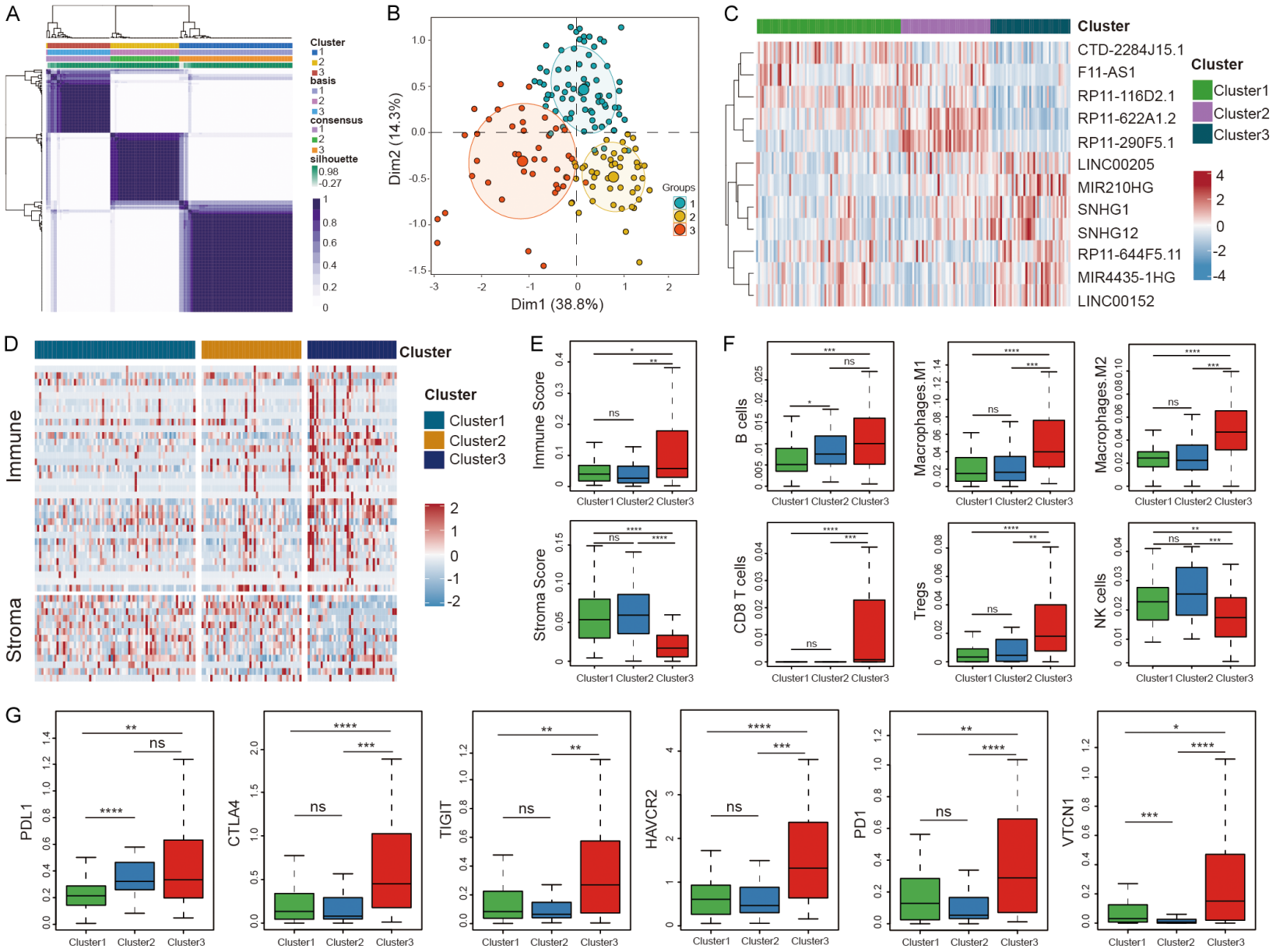
A
Cluster
basis
consensus
silhouette
B
Dim2 (14.3%)
Dim1 (38.8%)
Groups
C
Cluster
CTD-2284J15.1
F11-AS1
RP11-116D2.1
RP11-622A1.2
RP11-290F5.1
LINC00205
MIR210HG
SNHG1
SNHG12
RP11-644F5.11
MIR4435-1HG
LINC00152
Cluster1
Cluster2
Cluster3
D
Immune
Stroma
E
Immune Score
Stroma Score
F
B cells
Macrophages.M1
Macrophages.M2
CD8 T cells
Tregs
NK cells
G
PDL1
CTLA4
TIGIT
HAVCR2
PD1
VTCN1

Figure 6. Validation of the classification based on 12 lncRNAs in ICGC dataset. A. NMF clustering based on 12 m6A-LncRNAs in ICGC dataset. B. PCA analysis supported the stratification into three subclasses. C. Heatmap of the expression of the 12 lncRNAs in the three clusters. D. Heatmap of cell infiltration score calculated with the xCell algorithm. Red indicates higher score, blue indicates lower score. E, F. Comparison of immune score, stroma score and immune cell fraction between the three subclasses. G. Comparison of the expression of checkpoint genes in the three subclasses. Statistical significance of differences was determined by Wilcoxon rank-sum test. *, P < 0.05; **, P < 0.01; ***, P < 0.001; ****, P < 0.0001; ns, no significance.

(Cluster1 vs. Cluster2, no significance; Cluster1 vs. Cluster3, P < 0.0001; Cluster2 vs. Cluster3, p < 0.01) infiltration and lower NK cell (Cluster1 vs. Cluster2, no significance; Cluster1 vs. Cluster3, P < 0.01; Cluster2 vs. Cluster3, P < 0.001) infiltration than the other two clusters (**Figure 6F**). Then, we analyzed the exhaustion markers in the 3 clusters and found that these exhaustion marker genes had higher expression in Cluster3 (**Figure 6G**). Since HCC patients can be well distinguished based on the 12 m6A-LncRNAs in two large, independent cohorts, these results indicate that the 12 m6A-LncRNAs may play central roles in the regulation of the tumor microenvironment.

Relationships between m6A-LncRNAs and immune characteristics in HCC

The 12 m6A-LncRNA signatures showed frequent significant correlations with the m6A writers and readers, but not the erasers (**Figure 7A**). However, the specific roles of the 12 m6A-LncRNAs in the regulation of the immune response remain elusive. To further determine how m6A-LncRNAs influence the immune environment in HCC, we investigated correlations between m6A-LncRNAs and immune cells and immune regulatory genes as previously reported [30]. The m6A-LncRNAs were significantly correlated with the infiltration of immune cells and the immune regulatory genes (**Figure 7B** and **7C**). For instance, SNHG12 showed positive associations with infiltration of B cells, macrophages, $CD8^+$ T cells and Tregs, as well as the expression of RELT, CTLA4 and PD1 (P < 0.01).

The three clusters show distinct sensitivity to immune checkpoint blockades

Numerous studies have identified that tumor microenvironment factors influence the response to immunotherapy [31]. The differences in immune cell infiltration and immune checkpoint gene expression patterns among the three HCC subtypes indicated that the response to immunotherapy needs to be further investigated. The Tumor Immune Dysfunction and Exclusion (TIDE) score was used to assess immune evasion and exhaustion and reflect the efficacy of immunotherapy. A higher TIDE score reflects higher immune cell evasion and suggests less sensitivity to immune checkpoint inhibitors (ICIs). Compared with the other two clusters, the C3 (Cluster3) had higher TIDE scores in TCGA (C2 vs. C1, P < 0.01; C2 vs. C3, P < 0.0001; C1 vs. C3, P < 0.0001) and ICGC datasets (Cluster1 vs. Cluster2, no significance; Cluster1 vs. Cluster3, P < 0.001; Cluster2 vs. Cluster3, P < 0.001), indicating that patients in C3 were less likely to benefit from ICIs therapy (**Figure 8A**). A previous study demonstrated that the immunophenoscore (IPS) was a superior predictor of response to CTLA4 and PDL1 blockades [29]. As a result, C1 showed better responses to single CTLA4 blockades (C2 vs. C1, P < 0.01; C2 vs. C3, no significance; C1 vs. C3, P < 0.001) or PDL1 blockades (C2 vs. C1, P < 0.01; C2 vs. C3, no significance; C1 vs. C3, P < 0.001) and the combination of CTLA4 and PDL1 blockades (C2 vs. C1, P < 0.001; C2 vs. C3, no significance; C1 vs. C3, P < 0.01; **Figure 8B**). Furthermore, the expression profiles of the three subclasses and the published dataset, including the expression profiles of 47 melanoma patients who received PD-1 inhibitors or CTLA-4 inhibitors, were compared using a subclass mapping algorithm [32]. The expression profile of the C1 subtype was similar to that of the PD-1 response group (P=0.006, corrected P=0.08), indicating that patients in the C1 subgroup were more sensitive to ICIs therapy (**Figure 8C**). C3 exhibited significantly higher sensitivity to sorafenib (C2 vs. C1, P < 0.0001; C2 vs. C3, P < 0.001; C1 vs. C3, P < 0.0001) and AKT inhibitor (C2 vs. C1, p < 0.0001; C2 vs. C3, P < 0.0001; C1 vs. C3, P < 0.0001, **Figure 8D**).

Discussion

As the most abundant and critical form of internal RNA modification in eukaryotes, m6A modi-

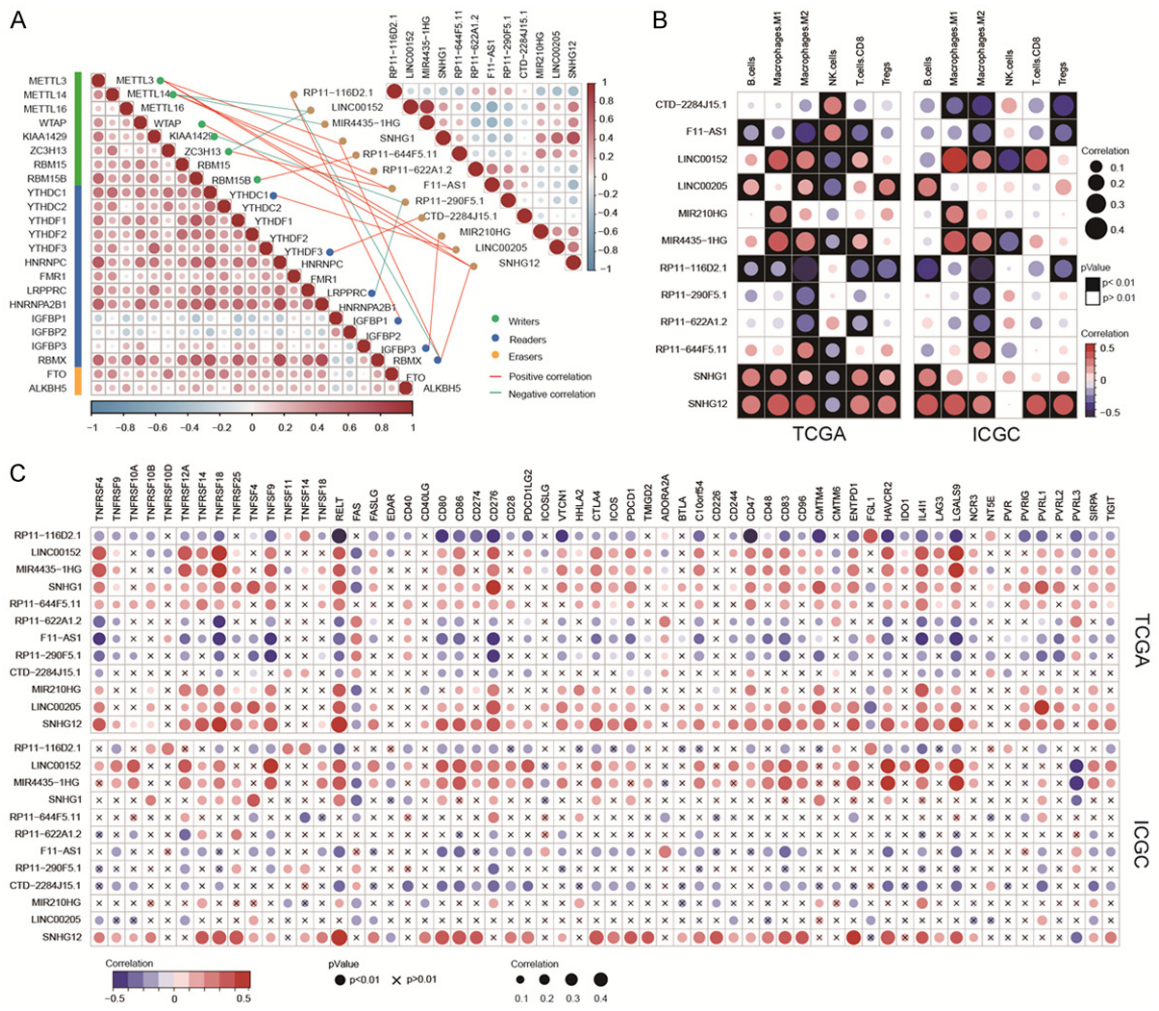

Figure 7. Relationship between m6A-related signatures and the immune characteristics. (A) Correlations between the 12 lncRNA signatures and m6A genes, (B) immune cells, and (C) immune checkpoints.

fication plays vital roles in multiple cellular processes. The interactions between m6A modification and lncRNAs influence various biological processes in tumor, including its occurrence, metastasis and chemoresistance [11]. In this integrated analysis, we identified 82 prognostic m6A-LncRNAs from the TCGA and ICGC datasets. Based on the expression profiles of these lncRNAs, HCC patients were classified into three subtypes with distinct clinical features, immune and stromal infiltration signatures, and predicted immunotherapy sensitivity.

Over the past few decades, a series of studies have proposed distinct criteria for a molecular-level classification of HCC subtypes. In 2007, Boyault et al. identified 6 HCC subclasses (G1-G6) typified by notable differences in chromosome instability, gene mutations, immune responses and metabolic pathways [33]. Later in 2008, through unsupervised cluster analysis of gene expression files from 91 HCC patients, Chiang et al. reported a classification scheme of the “CTNNB1”, “proliferation”, “IFN-related”, “Polysomy of chromosome 7” and “unannotated” HCC subclasses [34]. In 2009, Hoshida et al. observed 3 major molecular subtypes in HCC patients from Western and Eastern countries (S1-S3), which were distinguished by differences in activation of WNT and TGFB signaling pathways, proliferation and hepatocyte differentiation signatures [35]. In 2017, Sia et al. identified two major HCC subtypes that displayed the “immune” or “non-immune” characteristics. The “immune” group was further divided into the “active immune” and “exhausted

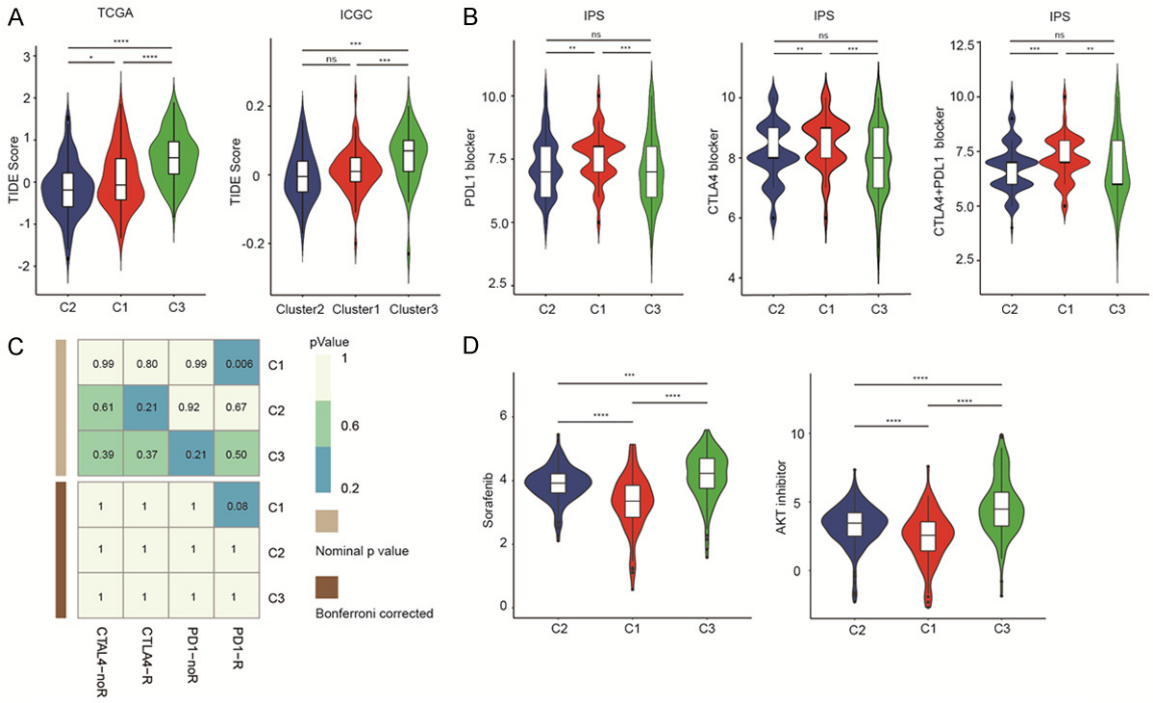

Figure 8. Immunotherapeutic sensitivity of the three subclasses. A, B. Comparison of tumor immune dysfunction and exclusion (TIDE) and Immunophenoscore (IPS) in the three HCC subclasses. C. Similarities between the three HCC subclasses and the dataset that received PD1 and CTLA4 inhibitors. D. Prediction of responses to Sorafenib and AKT inhibitor. Statistical significance of differences was determined by Wilcoxon rank-sum test. *, $p < 0.05$; **, $P < 0.01$; ***, $P < 0.001$; ****, $P < 0.0001$; ns, no significance.

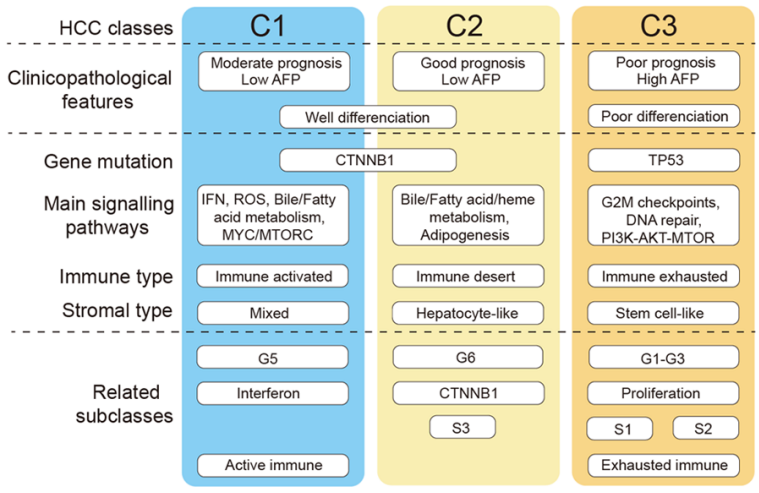

Figure 9. Overview of the characteristics of three HCC subclasses.

immune" subclasses [36]. However, an overarching agreement in molecular taxonomy of HCC has not been achieved.

Through literature review, we found C1 matched with the "G5", "IFN-related" and "active immune" subclasses for enriching in active immune responses. C2 showed similarities with "G6", "CTNNB1", "S3" and "non-immune" classes, which were characterized by good differentiation and favorable prognosis. C3 displayed high mutation frequency in TP53 and enriched in proliferation and suppressed immunity related pathways, matching the "G1-G3", "Proliferation", "S1, S2" and "exhausted immune" subclasses (**Figure 9**). The classification of HCC based on m6A-LncRNAs is comparable to the previous studies, indicating the critical functions of m6A-LncRNAs in HCC, especially in the regulation of immune environments. This also suggests that many of the earlier molecular classification schemes may have in fact arrived at similar conclusions in terms of stratification, just under different naming mechanisms.

Recent studies have revealed the association between m6A modification and immune cell

infiltration in the tumor microenvironment [37-39]. However, few studies have identified the possible interactions between m6A modification and lncRNAs in the regulation of the immune responses. We analyzed the correlation between m6A-LncRNAs and tumor-infiltrating cells and immune regulatory genes. Qian et al. demonstrated that lncRNA SNHG12 facilitates ovarian cancer escape by promoting IL-6/miR-21 crosstalk between ovarian cancer cells and M2 macrophages [40]. In our study, lncRNA SNHG12 showed significant positive correlation with the presence of M2 macrophages, indicating that m6A modification may take part in the regulation of SNGH12 and M2 macrophages, especially through the m6A regulatory genes METTL3, RBMX and WTAP, which showed significant correlations with SNHG12. Ou et al. found that in gastric cancer, LINC00152 is negatively correlated with $CD8^+$ T cells [41]. However, LINC00152 showed a significant positive correlation with $CD8^+$ T cells in HCC through our analysis, and the underlying mechanisms need to be uncovered. More generally, lncRNAs have been shown to be involved in tumor immune exhaustion [42]. LncRNA Tim3 exacerbates $CD8^+$ T cell exhaustion by binding to the immune checkpoint protein TIM3 [43]. The lncRNA KCNQ1OT1 regulates the expression of CD155 and mediates $CD8^+$ T cell exhaustion [44]. In this study, m6A-LncRNAs showed obvious correlations with T cell exhaustion markers. However, further experimental studies are warranted to delineate the corresponding mechanisms associated with m6A modification, lncRNAs and immune exhaustion.

Patients in C3 showed the highest expression of immune checkpoints but failed to respond to ICIs through our analysis. This suggested that in HCC, the expression of immune checkpoints on tumor cells may not be sufficient to predict the response to ICIs, and alternative predictive markers remain to be identified. This inference is consistent with a phase II study in which PD-L1 expression failed to be predictive of the response to nivolumab treatment for HCC patients [45]. Several biomarkers have been proposed in other cancer types, such as high levels of effector cell infiltration, increased secretion of interferon gamma, and high somatic TMB and neoantigen load [31]. In this study, neither the somatic TMB nor the neoantigen load was associated with the classification, suggesting that other mechanisms may influence the antitumor immune response in the 3 subclasses. C1 was highly enriched in IFNγ signaling pathways, reinforcing the opinion that the pre-existing IFN-related immune environment is required for the responses to PD-1 inhibitors [46]. Satisfactory responses to ICIs depend on the complicated interactions between stromal cells, immune cells and other immunomodulators. To promote the efficacy of immunotherapies, it is critical to uncover the interactions between the immune response and the tumor microenvironment. In this regard, the exhausted and suppressive immune subtype, namely C3 subtype in this study, may benefit from the combination of TGF-β inhibitors and ICIs. Currently, the combination of the TGF-β inhibitor galunisertib with nivolumab in treating advanced HCC is ongoing in a phase 2 clinical trial (NCT02423343) and the result is greatly anticipated. However, further clinical investigation in patients treated with ICIs and TGF-β inhibitors is needed to validate the predictive accuracy of our classifier.

In summary, we identified 82 prognostic m6A-LncRNAs in HCC, comprehensively evaluated the 3 distinct HCC subtypes classified by these lncRNAs, and systematically correlated these lncRNAs with tumor immune environment characteristics. This integrated analysis indicates that the interactions between m6A methylation and lncRNAs are involved in immune and stromal cell infiltration in HCC, and may provide novel insights into precision diagnostics as well as therapeutics for HCC patients.

Conclusion

In the current study, we identified 82 m6A-LncRNAs with prognostic significance in HCC and constructed an m6A-lncRNA regulatory network. Based on the expression of the prognostic m6A-LncRNAs, we discovered three molecular HCC subtypes with distinct clinical features, immune and stromal infiltration signatures and immunotherapy sensitivity. However, further experimental and clinical validations are warranted to delineate the corresponding mechanisms associated with m6A modification, lncRNAs and immunotherapy.

Acknowledgements

We are very grateful to the Cancer Genome Atlas (TCGA) database and International Cancer

Genome Consortium (ICGC) database for providing the transcriptome and clinical information. We thank Zihan Zheng for his kind suggestions.

Disclosure of conflict of interest

None.

Abbreviations

M6A, N6-methyladenosine; M6A-LncRNA, M6A-related lncRNA; HCC, Hepatocellular Carcinoma; TCGA, The Cancer Genome Atlas; ICGC, International Cancer Genome Consortium; OS, Overall Survival; DFS, Disease-Free Survival; AFP, Serum Alpha Fetoprotein; CYT, Cytolytic; TIS, Tumor Inflammation Score; TMB, Tumor Mutation Burden; CNV, Copy Number Variation; DEGs, Differentially Expressed Genes; PCA, Principal Component Analysis; TIDE, Tumor Immune Dysfunction and Exclusion; IPS, Immunophenoscore; ICIs, Immune Checkpoint Inhibitors; NMF, Nonnegative Matrix Factorization; GSVA, Geneset Variation Analysis; TME, Tumor Microenvironment.

Address correspondence to: Long Cheng and Tao Wang, Department of General Surgery, The General Hospital of Western Theater Command (Chengdu Military General Hospital), Chengdu 610083, Sichuan Province, China. Tel: +86-02886571003; E-mail: tmmulong@163.com (LC); watopo@163.com (TW)

References

[1] Sung H, Ferlay J, Siegel RL, Laversanne M, Soerjomataram I, Jemal A and Bray F. Global cancer statistics 2020: GLOBOCAN estimates of incidence and mortality worldwide for 36 cancers in 185 countries. CA Cancer J Clin 2021; 71: 209-249.

[2] Villanueva A. Hepatocellular carcinoma. N Engl J Med 2019; 380: 1450-1462.

[3] Kulik L and El-Serag HB. Epidemiology and management of hepatocellular carcinoma. Gastroenterology 2019; 156: 477-491, e471.

[4] Zhao BS, Roundtree IA and He C. Post-transcriptional gene regulation by mRNA modifications. Nat Rev Mol Cell Biol 2017; 18: 31-42.

[5] Zaccara S, Ries RJ and Jaffrey SR. Reading, writing and erasing mRNA methylation. Nat Rev Mol Cell Biol 2019; 20: 608-624.

[6] Wang T, Kong S, Tao M and Ju S. The potential role of RNA N6-methyladenosine in cancer progression. Mol Cancer 2020; 19: 88.

[7] Chen Y, Peng C, Chen J, Chen D, Yang B, He B, Hu W, Zhang Y, Liu H, Dai L, Xie H, Zhou L, Wu J and Zheng S. WTAP facilitates progression of hepatocellular carcinoma via m6A-HuR-dependent epigenetic silencing of ETS1. Mol Cancer 2019; 18: 127.

[8] Shi Y, Zhuang Y, Zhang J, Chen M and Wu S. METTL14 inhibits hepatocellular carcinoma metastasis through regulating EGFR/PI3K/AKT signaling pathway in an m6A-dependent manner. Cancer Manag Res 2020; 12: 13173-13184.

[9] Schmitt AM and Chang HY. Long noncoding RNAs in cancer pathways. Cancer Cell 2016; 29: 452-463.

[10] Zhao J and Lawless MW. Long noncoding RNAs and their role in the liver cancer axis. Nat Rev Gastroenterol Hepatol 2013; 10: 703.

[11] Lan Y, Liu B and Guo H. The role of M(6)A modification in the regulation of tumor-related lncRNAs. Mol Ther Nucleic Acids 2021; 24: 768-779.

[12] Zuo X, Chen Z, Gao W, Zhang Y, Wang J, Wang J, Cao M, Cai J, Wu J and Wang X. M6A-mediated upregulation of LINC00958 increases lipogenesis and acts as a nanotherapeutic target in hepatocellular carcinoma. J Hematol Oncol 2020; 13: 5.

[13] Xu F, Huang X, Li Y, Chen Y and Lin L. m(6)A-related lncRNAs are potential biomarkers for predicting prognoses and immune responses in patients with LUAD. Mol Ther Nucleic Acids 2021; 24: 780-791.

[14] Yang Y, Hsu PJ, Chen YS and Yang YG. Dynamic transcriptomic m(6)A decoration: writers, erasers, readers and functions in RNA metabolism. Cell Res 2018; 28: 616-624.

[15] Lee DD and Seung HS. Learning the parts of objects by non-negative matrix factorization. Nature 1999; 401: 788-791.

[16] Gaujoux R and Seoighe C. A flexible R package for nonnegative matrix factorization. BMC Bioinformatics 2010; 11: 367.

[17] Aran D, Hu Z and Butte AJ. xCell: digitally portraying the tissue cellular heterogeneity landscape. Genome Biol 2017; 18: 220.

[18] Plattner C, Finotello F and Rieder D. Deconvoluting tumor-infiltrating immune cells from RNA-seq data using quanTIseq. Methods Enzymol 2020; 636: 261-285.

[19] Danaher P, Warren S, Lu R, Samayoa J, Sullivan A, Pekker I, Wallden B, Marincola FM and Cesano A. Pan-cancer adaptive immune resistance as defined by the Tumor Inflammation Signature (TIS): results from The Cancer Genome Atlas (TCGA). J Immunother Cancer 2018; 6: 63.

[20] Hänzelmann S, Castelo R and Guinney J. GSVA: gene set variation analysis for microarray and

RNA-seq data. BMC Bioinformatics 2013; 14: 7.
[21] Love MI, Huber W and Anders S. Moderated estimation of fold change and dispersion for RNA-seq data with DESeq2. Genome Biol 2014; 15: 550.
[22] Zhou Y, Zhou B, Pache L, Chang M, Khodabakhshi AH, Tanaseichuk O, Benner C and Chanda SK. Metascape provides a biologist-oriented resource for the analysis of systems-level datasets. Nat Commun 2019; 10: 1523.
[23] Jiang P, Gu S, Pan D, Fu J, Sahu A, Hu X, Li Z, Traugh N, Bu X, Li B, Liu J, Freeman GJ, Brown MA, Wucherpfennig KW and Liu XS. Signatures of T cell dysfunction and exclusion predict cancer immunotherapy response. Nat Med 2018; 24: 1550-1558.
[24] Charoentong P, Finotello F, Angelova M, Mayer C, Efremova M, Rieder D, Hackl H and Trajanoski Z. Pan-cancer immunogenomic analyses reveal genotype-immunophenotype relationships and predictors of response to checkpoint blockade. Cell Rep 2017; 18: 248-262.
[25] Reich M, Liefeld T, Gould J, Lerner J, Tamayo P and Mesirov JP. GenePattern 2.0. Nat Genet 2006; 38: 500-501.
[26] Geeleher P, Cox NJ and Huang RS. Clinical drug response can be predicted using baseline gene expression levels and in vitro drug sensitivity in cell lines. Genome Biol 2014; 15: R47.
[27] Rizvi NA, Hellmann MD, Snyder A, Kvistborg P, Makarov V, Havel JJ, Lee W, Yuan J, Wong P, Ho TS, Miller ML, Rekhtman N, Moreira AL, Ibrahim F, Bruggeman C, Gasmi B, Zappasodi R, Maeda Y, Sander C, Garon EB, Merghoub T, Wolchok JD, Schumacher TN and Chan TA. Cancer immunology. Mutational landscape determines sensitivity to PD-1 blockade in non-small cell lung cancer. Science 2015; 348: 124-128.
[28] Dong ZY, Zhong WZ, Zhang XC, Su J, Xie Z, Liu SY, Tu HY, Chen HJ, Sun YL, Zhou Q, Yang JJ, Yang XN, Lin JX, Yan HH, Zhai HR, Yan LX, Liao RQ, Wu SP and Wu YL. Potential predictive value of TP53 and KRAS mutation status for response to PD-1 blockade immunotherapy in lung adenocarcinoma. Clin Cancer Res 2017; 23: 3012-3024.
[29] Finotello F, Mayer C, Plattner C, Laschober G, Rieder D, Hackl H, Krogsdam A, Loncova Z, Posch W, Wilflingseder D, Sopper S, Ijsselsteijn M, Brouwer TP, Johnson D, Xu Y, Wang Y, Sanders ME, Estrada MV, Ericsson-Gonzalez P, Charoentong P, Balko J, de Miranda N and Trajanoski Z. Molecular and pharmacological modulators of the tumor immune contexture revealed by deconvolution of RNA-seq data. Genome Med 2019; 11: 34.
[30] Zhang C, Zhang Z, Zhang Z, Luo Y, Wu P, Zhang G, Xue L, Zeng Q, Wang L, Yang Z, Zeng H, Zheng B, Tan F, Xue Q, Gao S, Sun N and He J. The landscape of m(6)A regulators in small cell lung cancer: molecular characteristics, immuno-oncology features, and clinical relevance. Mol Cancer 2021; 20: 122.
[31] Picard E, Verschoor CP, Ma GW and Pawelec G. Relationships between immune landscapes, genetic subtypes and responses to immunotherapy in colorectal cancer. Front Immunol 2020; 11: 369.
[32] Roh W, Chen PL, Reuben A, Spencer CN, Prieto PA, Miller JP, Gopalakrishnan V, Wang F, Cooper ZA, Reddy SM, Gumbs C, Little L, Chang Q, Chen WS, Wani K, De Macedo MP, Chen E, Austin-Breneman JL, Jiang H, Roszik J, Tetzlaff MT, Davies MA, Gershenwald JE, Tawbi H, Lazar AJ, Hwu P, Hwu WJ, Diab A, Glitza IC, Patel SP, Woodman SE, Amaria RN, Prieto VG, Hu J, Sharma P, Allison JP, Chin L, Zhang J, Wargo JA and Futreal PA. Integrated molecular analysis of tumor biopsies on sequential CTLA-4 and PD-1 blockade reveals markers of response and resistance. Sci Transl Med 2017; 9: eaah3560.
[33] Boyault S, Rickman DS, de Reyniès A, Balabaud C, Rebouissou S, Jeannot E, Hérault A, Saric J, Belghiti J, Franco D, Bioulac-Sage P, Laurent-Puig P and Zucman-Rossi J. Transcriptome classification of HCC is related to gene alterations and to new therapeutic targets. Hepatology 2007; 45: 42-52.
[34] Chiang DY, Villanueva A, Hoshida Y, Peix J, Newell P, Minguez B, LeBlanc AC, Donovan DJ, Thung SN, Solé M, Tovar V, Alsinet C, Ramos AH, Barretina J, Roayaie S, Schwartz M, Waxman S, Bruix J, Mazzaferro V, Ligon AH, Najfeld V, Friedman SL, Sellers WR, Meyerson M and Llovet JM. Focal gains of VEGFA and molecular classification of hepatocellular carcinoma. Cancer Res 2008; 68: 6779-6788.
[35] Hoshida Y, Nijman SM, Kobayashi M, Chan JA, Brunet JP, Chiang DY, Villanueva A, Newell P, Ikeda K, Hashimoto M, Watanabe G, Gabriel S, Friedman SL, Kumada H, Llovet JM and Golub TR. Integrative transcriptome analysis reveals common molecular subclasses of human hepatocellular carcinoma. Cancer Res 2009; 69: 7385-7392.
[36] Sia D, Jiao Y, Martinez-Quetglas I, Kuchuk O, Villacorta-Martin C, Castro de Moura M, Putra J, Camprecios G, Bassaganyas L, Akers N, Losic B, Waxman S, Thung SN, Mazzaferro V, Esteller M, Friedman SL, Schwartz M, Villanueva A and Llovet JM. Identification of an immune-specific class of hepatocellular carcinoma, based on molecular features. Gastroenterology 2017; 153: 812-826.

[37] Shulman Z and Stern-Ginossar N. The RNA modification N(6)-methyladenosine as a novel regulator of the immune system. Nat Immunol 2020; 21: 501-512.
[38] Yi L, Wu G, Guo L, Zou X and Huang P. Comprehensive analysis of the PD-L1 and immune infiltrates of m(6)A RNA methylation regulators in head and neck squamous cell carcinoma. Mol Ther Nucleic Acids 2020; 21: 299-314.
[39] Chong W, Shang L, Liu J, Fang Z, Du F, Wu H, Liu Y, Wang Z, Chen Y, Jia S, Chen L, Li L and Chen H. m(6)A regulator-based methylation modification patterns characterized by distinct tumor microenvironment immune profiles in colon cancer. Theranostics 2021; 11: 2201-2217.
[40] Qian M, Ling W and Ruan Z. Long non-coding RNA SNHG12 promotes immune escape of ovarian cancer cells through their crosstalk with M2 macrophages. Aging (Albany NY) 2020; 12: 17122-17136.
[41] Ou J, Lei P, Yang Z, Yang M, Luo L, Mo H, Luo G and He J. LINC00152 mediates CD8(+) T-cell infiltration in gastric cancer through binding to EZH2 and regulating the CXCL9, 10/CXCR3 axis. J Mol Histol 2021; 52: 611-620.
[42] Xu S, Wang Q, Kang Y, Liu J, Yin Y, Liu L, Wu H, Li S, Sui S, Shen M, Zheng W and Pang D. Long noncoding RNAs control the modulation of immune checkpoint molecules in cancer. Cancer Immunol Res 2020; 8: 937-951.
[43] Ji J, Yin Y, Ju H, Xu X, Liu W, Fu Q, Hu J, Zhang X and Sun B. Long non-coding RNA Lnc-Tim3 exacerbates CD8 T cell exhaustion via binding to Tim-3 and inducing nuclear translocation of Bat3 in HCC. Cell Death Dis 2018; 9: 478.
[44] Lin ZB, Long P, Zhao Z, Zhang YR, Chu XD, Zhao XX, Ding H, Huan SW, Pan YL and Pan JH. Long noncoding RNA KCNQ1OT1 is a prognostic biomarker and mediates CD8(+) T cell exhaustion by regulating CD155 expression in colorectal cancer. Int J Biol Sci 2021; 17: 1757-1768.
[45] El-Khoueiry AB, Sangro B, Yau T, Crocenzi TS, Kudo M, Hsu C, Kim TY, Choo SP, Trojan J, Welling TH Rd, Meyer T, Kang YK, Yeo W, Chopra A, Anderson J, Dela Cruz C, Lang L, Neely J, Tang H, Dastani HB and Melero I. Nivolumab in patients with advanced hepatocellular carcinoma (CheckMate 040): an open-label, non-comparative, phase 1/2 dose escalation and expansion trial. Lancet 2017; 389: 2492-2502.
[46] Ayers M, Lunceford J, Nebozhyn M, Murphy E, Loboda A, Kaufman DR, Albright A, Cheng JD, Kang SP, Shankaran V, Piha-Paul SA, Yearley J, Seiwert TY, Ribas A and McClanahan TK. IFN-γ-related mRNA profile predicts clinical response to PD-1 blockade. J Clin Invest 2017; 127: 2930-2940.

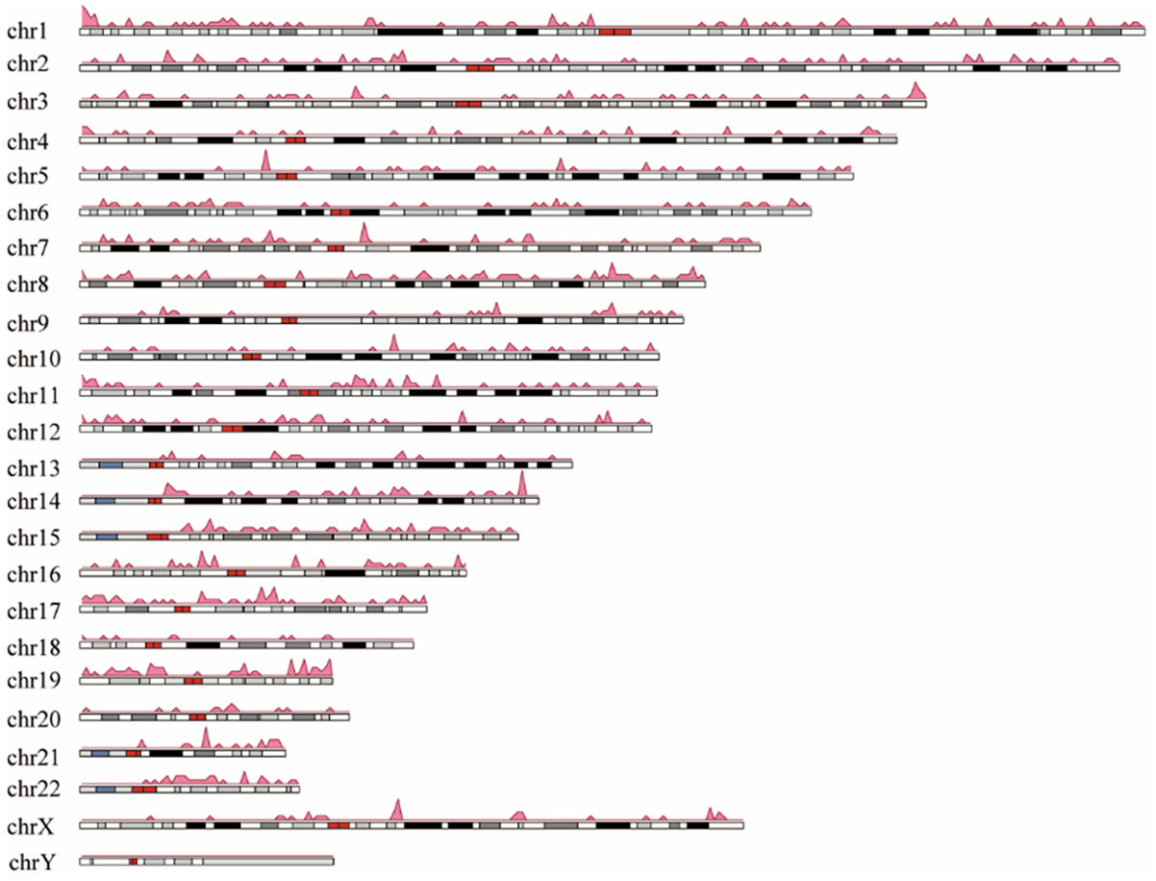

Figure S1. The locations of m6A-related lncRNAs (m6A-LncRNAs) on chromosomes.

Table S1. The prognistic m6a-related lncRNAs

LncRNAs	HR	z	*p* value	95%CI.lower	95%CI.upper	fdr	type
RP11-286H15.1	0.6682	-3.2443	0.0012	0.5238	0.8525	0.0233	protective
RP11-290F5.1	0.7258	-3.0804	0.0021	0.5919	0.89	0.0314	protective
F11-AS1	0.7355	-3.3442	0.0008	0.6143	0.8806	0.0181	protective
RP11-622A1.2	0.7378	-3.1545	0.0016	0.6108	0.8912	0.0268	protective
RP11-116D2.1	0.7452	-3.7369	0.0002	0.6387	0.8695	0.0093	protective
CTD-2284J15.1	0.7586	-2.9332	0.0034	0.6308	0.9124	0.0419	protective
RP11-395G23.3	1.2121	3.1694	0.0015	1.0762	1.3652	0.0265	risk
RP5-1024N4.4	1.2376	2.8362	0.0046	1.0681	1.434	0.0473	risk
RP11-452H21.4	1.2435	2.8709	0.0041	1.0716	1.4429	0.0446	risk
CTD-2201E18.5	1.2482	3.3306	0.0009	1.0955	1.4221	0.0181	risk
RP4-798A10.2	1.252	2.958	0.0031	1.0788	1.453	0.0403	risk
RP11-332H14.2	1.2538	2.9723	0.003	1.0801	1.4555	0.0394	risk
RP11-757F18.5	1.259	3.4324	0.0006	1.1039	1.436	0.0154	risk
RP11-15E18.1	1.2596	2.895	0.0038	1.0774	1.4727	0.0436	risk
RP11-461M2.2	1.2604	4.1657	0	1.1304	1.4055	0.0025	risk
RP11-398K22.12	1.2628	2.9464	0.0032	1.0812	1.4748	0.0408	risk
AC002116.7	1.2654	2.9844	0.0028	1.0842	1.4769	0.0394	risk
RP11-968A15.2	1.2657	2.8728	0.0041	1.0778	1.4865	0.0446	risk
MFI2-AS1	1.2673	2.8865	0.0039	1.079	1.4884	0.0441	risk

RP11-649A18.4	1.2692	2.9191	0.0035	1.0815	1.4895	0.0429	risk
RP11-148K1.12	1.2704	2.8543	0.0043	1.0779	1.4974	0.0458	risk
RP11-540A21.2	1.2714	3.6986	0.0002	1.1195	1.4439	0.0097	risk
RP11-95D17.1	1.2728	2.8367	0.0046	1.0774	1.5037	0.0473	risk
RP11-486G15.2	1.2739	2.9041	0.0037	1.0819	1.5	0.0436	risk
RP11-506M12.1	1.2739	2.9785	0.0029	1.0863	1.4939	0.0394	risk
AC005534.8	1.2754	2.8978	0.0038	1.0819	1.5036	0.0436	risk
BACH1-AS1	1.2761	2.9546	0.0031	1.0855	1.5002	0.0403	risk
RP11-474G23.3	1.2775	2.8947	0.0038	1.0823	1.508	0.0436	risk
BX322557.10	1.2794	2.8752	0.004	1.0816	1.5133	0.0446	risk
PTOV1-AS1	1.2813	2.9713	0.003	1.088	1.5089	0.0394	risk
RP11-199F11.2	1.2818	3.0664	0.0022	1.0937	1.5022	0.0323	risk
RP11-739N20.2	1.2823	3.049	0.0023	1.0929	1.5046	0.0325	risk
LINC00862	1.2869	3.3284	0.0009	1.1093	1.493	0.0181	risk
HCG15	1.2872	3.0611	0.0022	1.0951	1.513	0.0323	risk
RP11-884K10.7	1.2892	2.8641	0.0042	1.0835	1.5341	0.045	risk
RP11-383J24.1	1.2948	4.3891	0	1.1537	1.4532	0.0014	risk
RP11-343L5.2	1.296	3.0511	0.0023	1.0971	1.5308	0.0325	risk
RP11-108L7.15	1.2968	3.5899	0.0003	1.1252	1.4944	0.0108	risk
RP11-656D10.6	1.2996	3.1723	0.0015	1.1053	1.528	0.0265	risk
RP11-111M22.4	1.3013	3.3015	0.001	1.113	1.5216	0.0195	risk
SNHG12	1.3015	3.1127	0.0019	1.1025	1.5363	0.0292	risk
AC010761.8	1.3039	3.1882	0.0014	1.1076	1.5349	0.0259	risk
CTA-989H11.1	1.3048	3.0869	0.002	1.102	1.5449	0.0313	risk
AC016747.3	1.306	3.2018	0.0014	1.1091	1.5378	0.0252	risk
AC092168.2	1.3062	3.395	0.0007	1.1195	1.5239	0.0162	risk
CITF22-1A6.3	1.3073	3.139	0.0017	1.1059	1.5455	0.0277	risk
ZBTB11-AS1	1.3091	2.9174	0.0035	1.0924	1.5687	0.0429	risk
AC007405.4	1.3135	3.8735	0.0001	1.1442	1.5078	0.0061	risk
RP11-379B18.5	1.3148	3.4562	0.0005	1.1258	1.5356	0.0154	risk
TRAF3IP2-AS1	1.3153	3.1211	0.0018	1.1073	1.5624	0.0289	risk
AC074117.10	1.3193	3.1553	0.0016	1.1107	1.5671	0.0268	risk
RP11-809O17.1	1.3205	3.6061	0.0003	1.1353	1.5358	0.0106	risk
NDUFB2-AS1	1.3246	3.3849	0.0007	1.1256	1.5588	0.0164	risk
RP11-46F15.2	1.3254	3.4814	0.0005	1.131	1.5533	0.0146	risk
MIR4435-1HG	1.3275	3.4085	0.0007	1.1279	1.5623	0.0159	risk
RP11-428J1.5	1.3301	3.4353	0.0006	1.1303	1.5652	0.0154	risk
RP11-649A18.5	1.3304	3.4368	0.0006	1.1305	1.5656	0.0154	risk
CTD-2152M20.2	1.3307	3.6274	0.0003	1.1403	1.5527	0.0101	risk
RP11-527J8.1	1.337	3.2221	0.0013	1.1205	1.5953	0.0246	risk
SNHG1	1.3414	3.2114	0.0013	1.1213	1.6048	0.025	risk
LINC00205	1.3444	3.414	0.0006	1.1343	1.5934	0.0159	risk
RP11-432J22.2	1.3461	3.9397	0.0001	1.1611	1.5605	0.0058	risk
RP11-403I13.8	1.3463	3.6487	0.0003	1.1476	1.5796	0.0101	risk
CTD-2574D22.4	1.3518	3.5273	0.0004	1.1433	1.5983	0.0127	risk
GHRLOS	1.3543	3.6991	0.0002	1.1533	1.5905	0.0097	risk
RP11-152N13.5	1.3589	3.5741	0.0004	1.1485	1.6077	0.0111	risk
RHPN1-AS1	1.3596	3.8166	0.0001	1.1612	1.5919	0.0072	risk
RP11-274H2.5	1.3604	4.157	0	1.1766	1.5728	0.0025	risk

MCM3AP-AS1	1.3611	3.6393	0.0003	1.1529	1.6069	0.0101	risk
RP5-994D16.9	1.3628	3.3299	0.0009	1.1358	1.6352	0.0181	risk
BMS1P20	1.3647	3.675	0.0002	1.1562	1.6108	0.0101	risk
LINC00152	1.3649	3.8768	0.0001	1.1663	1.5974	0.0061	risk
RP6-65G23.3	1.3756	3.8871	0.0001	1.1713	1.6156	0.0061	risk
CTD-2199O4.6	1.3784	4.1891	0	1.1862	1.6016	0.0025	risk
RP11-4C20.4	1.3787	4.8143	0	1.2097	1.5713	0.0005	risk
CTD-2116N20.1	1.3793	4.229	0	1.1883	1.6009	0.0025	risk
RP11-644F5.11	1.4029	3.6493	0.0003	1.1697	1.6827	0.0101	risk
LL22NC03-N64E9.1	1.4236	5.6751	0	1.2601	1.6082	0	risk
DDX11-AS1	1.4359	4.5674	0	1.2294	1.6771	0.0007	risk
MIR210HG	1.452	4.7532	0	1.245	1.6934	0.0005	risk
RP11-417L19.4	1.4571	4.7081	0	1.2457	1.7043	0.0005	risk
RP11-324I22.4	1.498	4.6575	0	1.2637	1.7756	0.0005	risk

Table S2. The correlation between m6A genes and prognostic m6A-related lncRNAs

m6A gene	LncRNA	pval.tcga	cor.tcga	pval.icgc	cor.icgc
METTL3	RP11-46F15.2	3.27E-16	0.40670918	2.58E-09	0.44779777
METTL3	RP4-798A10.2	1.66E-21	0.467124722	4.89E-05	0.314321992
METTL3	SNHG12	1.65E-12	0.355750619	1.67E-07	0.398341795
METTL3	RP5-1024N4.4	4.03E-14	0.379029527	5.59E-07	0.382317619
METTL3	RP11-486G15.2	1.15E-14	0.386473519	5.11E-08	0.413195681
METTL3	AC074117.10	1.79E-26	0.514615114	9.81E-10	0.458249876
METTL3	RP11-474G23.3	4.32E-14	0.378612133	3.98E-07	0.386903767
METTL3	RP11-527J8.1	2.26E-31	0.555107885	2.83E-07	0.391449662
METTL3	RP11-332H14.2	3.32E-24	0.493834796	8.37E-14	0.544393424
METTL3	AC007405.4	4.31E-16	0.405187211	4.26E-06	0.353401379
METTL3	GHRLOS	1.52E-12	0.356292606	4.45E-10	0.46650844
METTL3	RP11-379B18.5	4.03E-13	0.364816512	3.69E-07	0.387913325
METTL3	MFI2-AS1	9.35E-10	0.310881639	4.68E-07	0.384730523
METTL3	CTD-2199O4.6	2.14E-11	0.338466266	1.49E-08	0.427963757
METTL3	CTD-2201E18.5	1.71E-10	0.323650015	4.76E-11	0.488781895
METTL3	CTD-2116N20.1	1.30E-15	0.399033908	7.13E-07	0.379001269
METTL3	RP11-343L5.2	2.98E-12	0.351847707	0.000107849	0.30043394
METTL3	TRAF3IP2-AS1	8.14E-26	0.508729082	7.73E-08	0.408068275
METTL3	RP11-506M12.1	3.81E-27	0.520498242	2.81E-07	0.391545158
METTL3	RP11-148K1.12	1.89E-11	0.339318917	7.76E-06	0.344276843
METTL3	AC005534.8	1.38E-09	0.307863899	3.81E-06	0.355040754
METTL3	RP11-432J22.2	4.78E-17	0.417079064	2.11E-05	0.328355097
METTL3	RP11-324I22.4	7.47E-15	0.389023123	1.63E-06	0.367414162
METTL3	RP11-152N13.5	2.68E-21	0.464964513	1.63E-10	0.476739992
METTL3	SNHG1	3.31E-28	0.529571759	4.47E-09	0.441725325
METTL3	RP11-111M22.4	1.10E-13	0.372937421	3.86E-10	0.467992523
METTL3	RP11-452H21.4	1.12E-17	0.424682793	1.86E-09	0.451406294
METTL3	CTD-2574D22.4	1.04E-28	0.533771495	3.12E-07	0.390128889
METTL3	RP11-199F11.2	2.30E-13	0.368352538	2.33E-19	0.632329111
METTL3	RP11-15E18.1	8.85E-18	0.42589215	6.52E-06	0.346949018
METTL3	RP11-649A18.5	1.47E-14	0.385053607	1.83E-05	0.330710668

METTL3	RP11-649A18.4	8.88E-13	0.359759546	8.07E-05	0.305622066
METTL3	AC002116.7	1.22E-09	0.308818739	1.90E-06	0.365208464
METTL3	BX322557.10	1.42E-23	0.487798768	9.77E-07	0.374653792
METTL3	LINC00205	1.10E-22	0.479067562	1.25E-06	0.371183919
METTL3	BMS1P20	1.27E-28	0.533040583	2.11E-07	0.395306393
METTL3	CITF22-1A6.3	3.84E-14	0.379324129	3.64E-08	0.417339026
METTL14	LINC00152	1.27E-15	-0.399184192	1.67E-12	-0.519394498
METTL14	MIR4435-1HG	1.28E-11	-0.342029406	5.66E-10	-0.464016405
METTL14	RP11-622A1.2	6.99E-11	0.330118228	2.27E-09	0.449198487
METTL14	F11-AS1	1.15E-13	0.372619813	2.70E-05	0.324359226
METTL16	RP11-95D17.1	5.23E-13	0.363156821	1.53E-06	0.36834138
WTAP	SNHG12	6.92E-22	0.471028658	2.94E-07	0.390948569
WTAP	RP11-403I13.8	1.68E-23	0.487100563	5.17E-07	0.383386522
WTAP	AC092168.2	1.19E-11	0.342506996	6.08E-05	0.310570078
WTAP	RP11-757F18.5	1.88E-13	0.369587166	1.49E-07	0.39979505
WTAP	CTD-2116N20.1	2.22E-18	0.432935659	6.79E-05	0.308638739
WTAP	TRAF3IP2-AS1	1.57E-34	0.57855535	2.19E-06	0.363176284
WTAP	RP11-395G23.3	6.44E-10	0.313732363	8.99E-05	0.303688233
WTAP	RP11-4C20.4	1.05E-11	0.343371328	1.49E-06	0.368708825
WTAP	DDX11-AS1	1.68E-19	0.445639025	2.57E-05	0.325156217
WTAP	RP11-649A18.5	3.23E-22	0.474386785	2.61E-06	0.360638111
WTAP	RP11-649A18.4	6.21E-21	0.461141708	0.000105786	0.300781884
KIAA1429	RP11-290F5.1	1.08E-16	-0.412723182	7.15E-06	-0.345520711
KIAA1429	CTD-2284J15.1	6.16E-14	0.376466698	5.92E-08	0.411379221
KIAA1429	RP11-383J24.1	9.02E-12	0.344415547	2.13E-06	0.363558905
KIAA1429	RHPN1-AS1	3.62E-22	0.473894186	4.70E-06	0.351903814
ZC3H13	LINC00152	1.32E-16	-0.411655969	1.35E-05	-0.335565573
ZC3H13	F11-AS1	1.64E-09	0.306532259	6.39E-05	0.309724321
RBM15	RP11-649A18.4	2.19E-10	0.321820523	8.60E-05	0.304488206
RBM15B	ZBTB11-AS1	4.24E-26	0.511273308	1.51E-09	0.453668874
RBM15B	RP11-428J1.5	1.83E-16	0.409868837	1.87E-08	0.425291431
RBM15B	NDUFB2-AS1	2.08E-15	0.396371067	0.000106472	0.300665512
RBM15B	RP11-540A21.2	1.69E-15	0.397572827	6.29E-05	0.309998659
RBM15B	RP11-644F5.11	1.28E-13	0.371974147	2.06E-06	0.36403748
RBM15B	RP6-65G23.3	8.35E-21	0.459780118	9.37E-05	0.302958461
RBM15B	CTA-989H11.1	2.47E-11	0.337485167	2.06E-07	0.395569734
YTHDC1	RP11-656D10.6	4.37E-19	0.440991895	1.10E-07	0.403587316
YTHDC1	RP11-527J8.1	1.89E-27	0.523134621	5.69E-05	0.311733085
YTHDC1	RP11-332H14.2	3.13E-31	0.5540097	1.51E-05	0.333802971
YTHDC1	RP11-884K10.7	3.89E-33	0.568441166	6.76E-05	0.308723509
YTHDC1	RP11-379B18.5	1.71E-09	0.306210972	3.26E-05	0.321193032
YTHDC1	TRAF3IP2-AS1	3.12E-22	0.474539759	1.94E-06	0.364895984
YTHDC1	PTOV1-AS1	2.91E-24	0.494379324	2.94E-05	0.322922934
YTHDC1	LINC00205	9.38E-23	0.479767682	3.83E-05	0.318476033
YTHDC2	RP11-332H14.2	1.96E-12	0.354607764	5.47E-07	0.382611922
YTHDF1	RP11-417L19.4	8.12E-15	0.388533167	3.31E-05	0.320931573
YTHDF2	RP5-994D16.9	1.37E-18	0.435359005	3.29E-07	0.389448172
YTHDF2	AC010761.8	4.81E-10	0.315939843	0.000103003	0.301261347
YTHDF2	BACH1-AS1	1.31E-13	0.371828997	1.27E-09	0.455528746

YTHDF3	CTD-2284J15.1	3.27E-18	0.430973468	1.07E-15	0.5774307
HNRNPC	RP5-994D16.9	3.56E-11	0.334920019	2.48E-05	0.325711914
HNRNPC	RP11-968A15.2	1.10E-15	0.399980913	5.09E-05	0.313649333
HNRNPC	BACH1-AS1	4.86E-10	0.315860105	1.54E-05	0.333482296
HNRNPC	LL22NC03-N64E9.1	5.89E-13	0.362395591	1.77E-07	0.39755783
LRPPRC	AC016747.3	1.94E-23	0.486488788	6.66E-05	0.308986755
LRPPRC	RP11-286H15.1	3.26E-09	-0.301109773	1.25E-06	-0.371145147
LRPPRC	RP11-290F5.1	5.63E-15	-0.39066811	7.93E-05	-0.305931945
LRPPRC	RP11-428J1.5	2.67E-16	0.407826684	2.03E-08	0.424304362
HNRNPA2B1	RP11-739N20.2	1.00E-28	0.533896758	8.50E-07	0.376575435
HNRNPA2B1	RP11-527J8.1	7.79E-33	0.566201402	5.87E-05	0.311197798
HNRNPA2B1	RP11-332H14.2	1.70E-32	0.563678236	1.17E-06	0.372178586
HNRNPA2B1	CTD-2152M20.2	1.83E-13	0.369753571	2.01E-05	0.329156388
HNRNPA2B1	RP11-432J22.2	1.62E-12	0.355872502	5.27E-05	0.313036005
HNRNPA2B1	RP11-108L7.15	2.71E-14	0.381423388	6.52E-05	0.309361545
HNRNPA2B1	RP11-452H21.4	2.59E-09	0.302918645	1.35E-06	0.370144401
HNRNPA2B1	DDX11-AS1	6.55E-27	0.518449205	0.000107413	0.300507031
HNRNPA2B1	RP11-649A18.5	1.40E-17	0.423513649	1.45E-05	0.334479997
IGFBP1	RP11-116D2.1	2.10E-17	0.421416472	1.02E-07	0.404566137
IGFBP3	LINC00862	6.84E-13	0.361437334	4.84E-05	0.314496033
IGFBP3	RP11-274H2.5	3.43E-10	0.31848898	9.53E-06	0.34107235
IGFBP3	MIR210HG	2.86E-16	0.407442736	1.77E-08	0.425958291
RBMX	SNHG12	2.46E-27	0.522134661	2.05E-07	0.395661615
RBMX	RP11-116D2.1	1.97E-30	-0.547754318	5.52E-06	-0.349472301
RBMX	RP11-527J8.1	1.32E-27	0.524465293	7.83E-07	0.377710504
RBMX	RP11-332H14.2	2.43E-26	0.513424613	6.71E-06	0.346511572
RBMX	RP11-461M2.2	6.72E-10	0.313414251	1.95E-05	0.32971481
RBMX	CTD-2199O4.6	4.89E-16	0.404492273	1.20E-08	0.430521258
RBMX	CTD-2116N20.1	2.64E-31	0.55458355	8.52E-06	0.342827336
RBMX	HCG15	1.66E-22	0.477295196	1.75E-06	0.366423709
RBMX	RP11-398K22.12	2.07E-25	0.505049244	2.88E-05	0.323242455
RBMX	TRAF3IP2-AS1	3.24E-33	0.569029893	5.56E-06	0.349372965
RBMX	RP11-809O17.1	1.55E-12	0.356142583	9.88E-06	0.340511256
RBMX	SNHG1	1.09E-52	0.684957184	9.42E-10	0.45868105
RBMX	RP11-111M22.4	1.03E-19	0.448002016	1.35E-05	0.335639503
RBMX	DDX11-AS1	1.89E-31	0.555709692	4.93E-06	0.351200859
RBMX	BX322557.10	3.46E-29	0.537712612	4.76E-06	0.351728229
RBMX	LINC00205	4.84E-39	0.609084761	6.35E-09	0.437782162
RBMX	MCM3AP-AS1	4.20E-40	0.615810056	1.18E-05	0.337753527

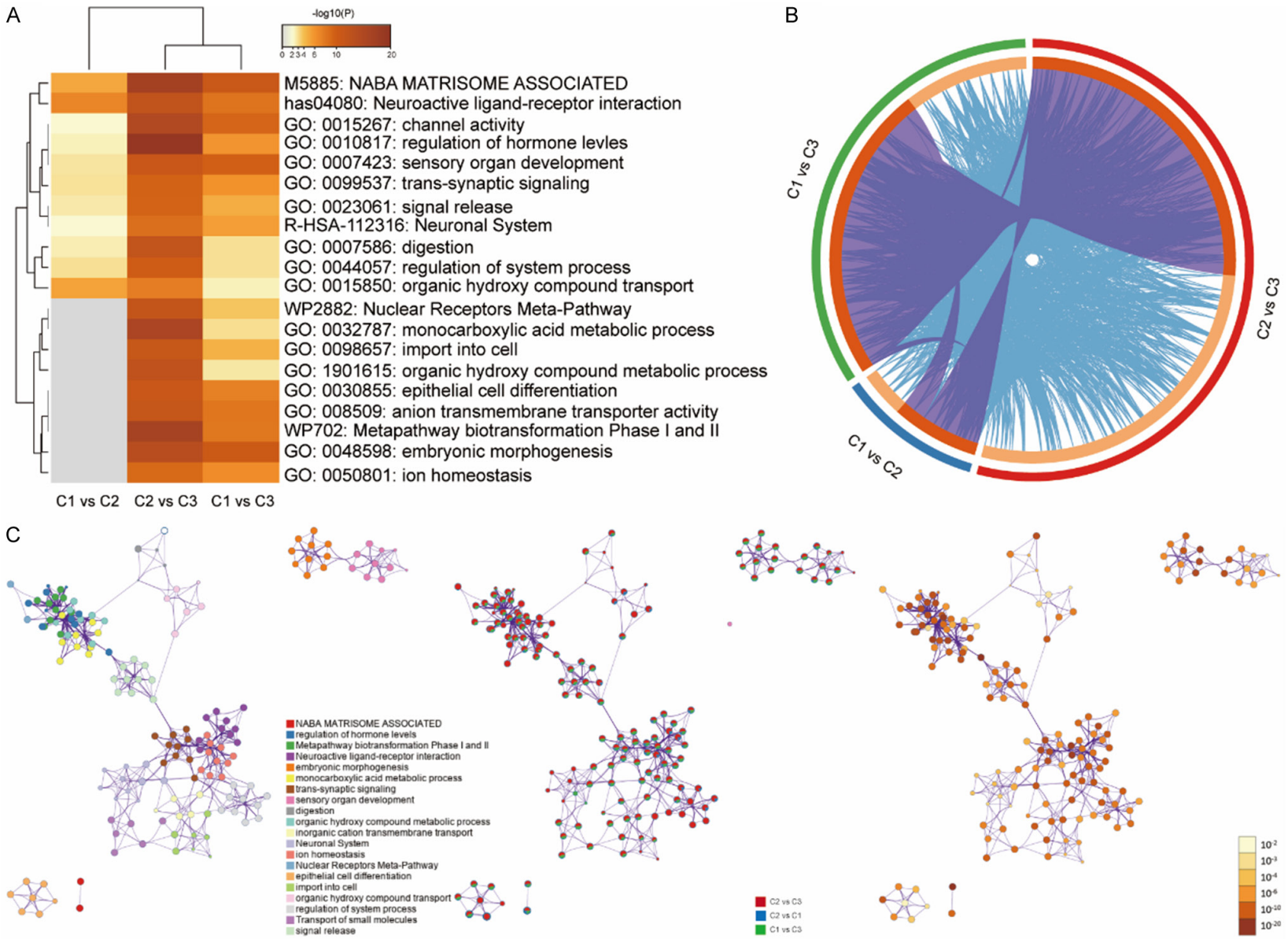
A
-log10(P)
0 2 3 4 6 10 20
M5885: NABA MATRISOME ASSOCIATED
has04080: Neuroactive ligand-receptor interaction
GO: 0015267: channel activity
GO: 0010817: regulation of hormone levles
GO: 0007423: sensory organ development
GO: 0099537: trans-synaptic signaling
GO: 0023061: signal release
R-HSA-112316: Neuronal System
GO: 0007586: digestion
GO: 0044057: regulation of system process
GO: 0015850: organic hydroxy compound transport
WP2882: Nuclear Receptors Meta-Pathway
GO: 0032787: monocarboxylic acid metabolic process
GO: 0098657: import into cell
GO: 1901615: organic hydroxy compound metabolic process
GO: 0030855: epithelial cell differentiation
GO: 008509: anion transmembrane transporter activity
WP702: Metapathway biotransformation Phase I and II
GO: 0048598: embryonic morphogenesis
GO: 0050801: ion homeostasis
C1 vs C2
C2 vs C3
C1 vs C3
B
C1 vs C3
C2 vs C3
C1 vs C2
C
NABA MATRISOME ASSOCIATED
regulation of hormone levels
Metapathway biotransformation Phase I and II
Neuroactive ligand-receptor interaction
embryonic morphogenesis
monocarboxylic acid metabolic process
trans-synaptic signaling
sensory organ development
digestion
organic hydroxy compound metabolic process
inorganic cation transmembrane transport
Neuronal System
ion homeostasis
Nuclear Receptors Meta-Pathway
epithelial cell differentiation
import into cell
organic hydroxy compound transport
regulation of system process
Transport of small molecules
signal release
C2 vs C3
C2 vs C1
C1 vs C3
10-2
10-3
10-4
10-6
10-10
10-20

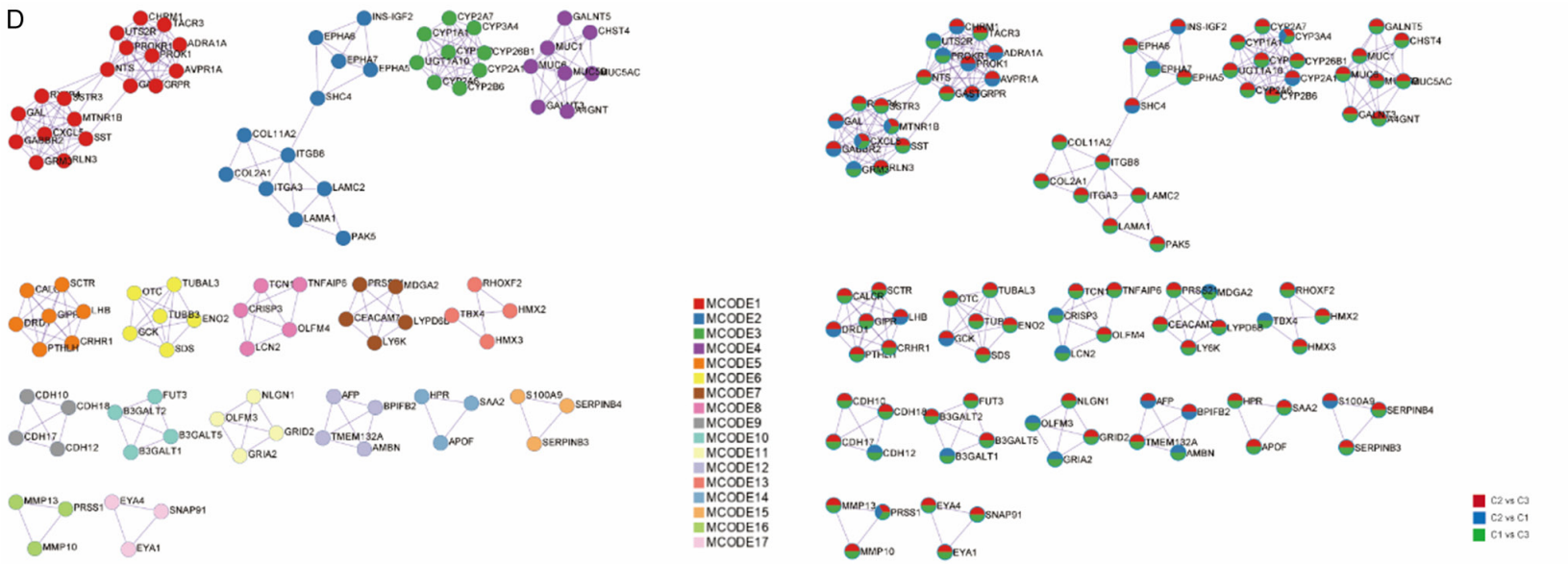

Figure S2. Functional enrichment of the differentially expressed genes (DEGs) between the three subclasses using Metascape. A. Heatmap of the enriched terms of the DEGs between the three subclasses (C1 vs. C2, C2 vs. C3, C1 vs. C3). B. Circle plot of the overlapping DEGs and enriched terms. C. Network of the enriched terms colored by cluster, *p*-value and counts. D. Protein-protein interaction network colored by cluster and counts.

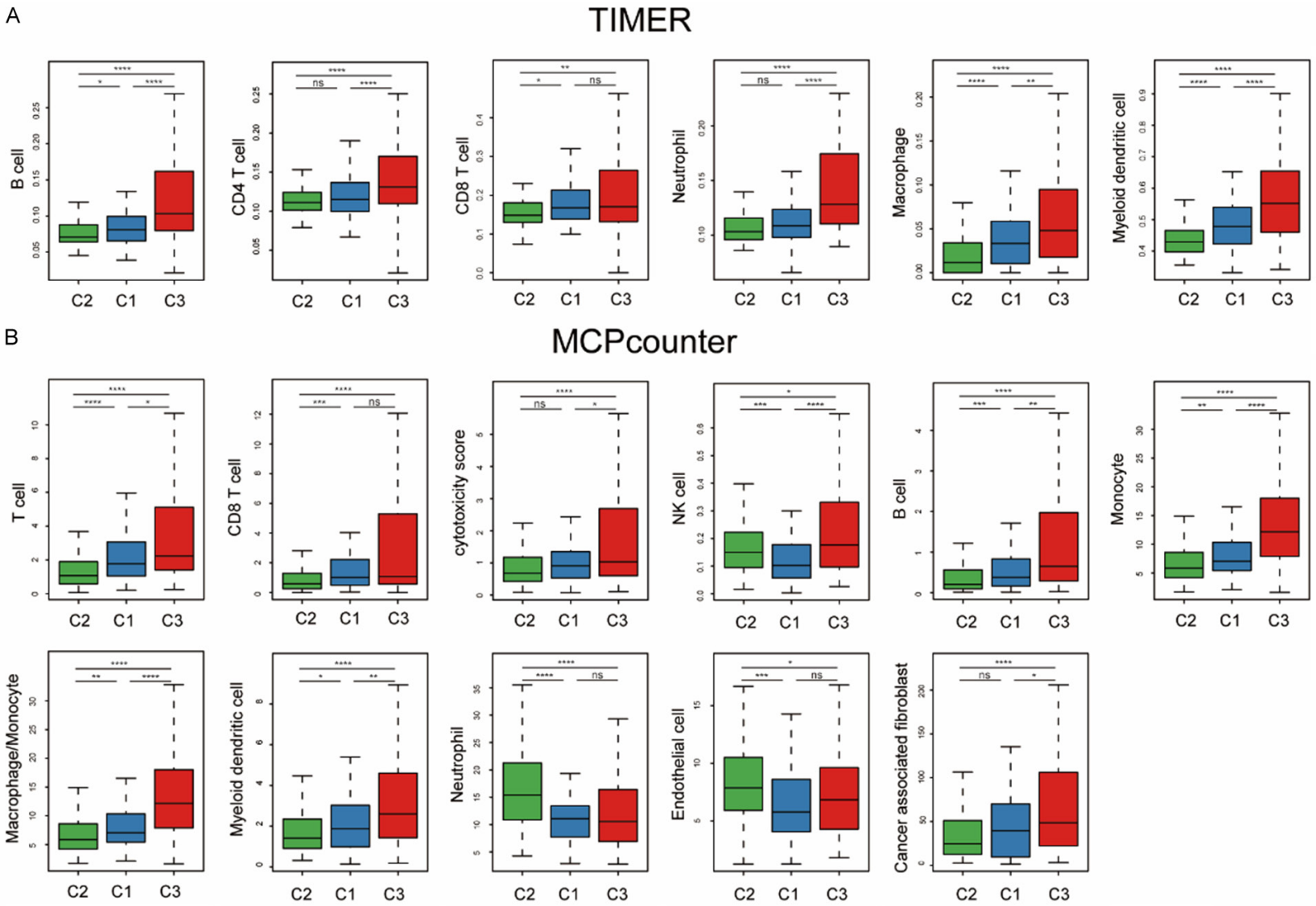

Figure S3. Tumor microenvironment (TME) characterization by TIMER (A) and MCPcounter (B). Statistical significance of differences was determined by Wilcoxon rank-sum test. *, P < 0.05; **, P < 0.01; ***, P < 0.001; ****, P < 0.0001; ns, no significance.